NAVAL POSTGRADUATE SCHOOL

MONTEREY, CALIFORNIA

THESIS

CLUTTER-COMPENSATING ADAPTIVE WAVEFORMS WITH COGNITIVE RADAR USING ACTUAL TARGET MEASUREMENTS FOR TARGET CLASSIFICATION

by

Ben Muwei Bey

September 2019

Thesis Advisor: Ric Romero
Second Reader: David C. Jenn

THIS PAGE INTENTIONALLY LEFT BLANK

REPORT DOCUMENTATION PAGE	*Form Approved OMB No. 0704-0188*

1. AGENCY USE ONLY *(Leave blank)*	**2. REPORT DATE** September 2019	**3. REPORT TYPE AND DATES COVERED** Master's thesis

4. TITLE AND SUBTITLE
CLUTTER-COMPENSATING ADAPTIVE WAVEFORMS WITH COGNITIVE RADAR USING ACTUAL TARGET MEASUREMENTS FOR TARGET CLASSIFICATION

5. FUNDING NUMBERS

6. AUTHOR(S) Ben Muwei Bey

7. PERFORMING ORGANIZATION NAME(S) AND ADDRESS(ES)
Naval Postgraduate School
Monterey, CA 93943-5000

8. PERFORMING ORGANIZATION REPORT NUMBER

9. SPONSORING / MONITORING AGENCY NAME(S) AND ADDRESS(ES)
N/A

10. SPONSORING / MONITORING AGENCY REPORT NUMBER

11. SUPPLEMENTARY NOTES The views expressed in this thesis are those of the author and do not reflect the official policy or position of the Department of Defense or the U.S. Government.

12a. DISTRIBUTION / AVAILABILITY STATEMENT	**12b. DISTRIBUTION CODE**
Approved for public release. Distribution is unlimited.	A

13. ABSTRACT (maximum 200 words)

In this work, we investigate the target classification performance of a cognitive radar (CRr) using EM-simulated ground-based target responses and EM-measured aerial target responses in the presence of transmit waveform-dependent clutter. Moreover, we consider a more realistic target classification scenario where the cognitive radar is pointing at a look angle of 30°, in which clutter can definitely be a major interference. Previous works included EM-simulated target responses with an adaptive waveform design technique known as probability-weighted energy (PWE) for target recognition; however, practically measured power spectrum density (PSD) for signal-dependent clutter was not considered. Therefore, it is essential to build on prior works by considering signal-dependent clutter using measured target responses and a practical clutter model. We design clutter-compensating adaptive waveforms for CRr to improve classification in the presence of both narrowband and wideband clutter. Our results show improvement in classification performance of clutter-mitigating SNR and MI-based waveforms used in conjunction with PWE.

14. SUBJECT TERMS	**15. NUMBER OF PAGES**
cognitive radar, waveform design, mutual information, target classification, clutter	71
	16. PRICE CODE

17. SECURITY CLASSIFICATION OF REPORT	**18. SECURITY CLASSIFICATION OF THIS PAGE**	**19. SECURITY CLASSIFICATION OF ABSTRACT**	**20. LIMITATION OF ABSTRACT**
Unclassified	Unclassified	Unclassified	UU

NSN 7540-01-280-5500

Standard Form 298 (Rev. 2-89)
Prescribed by ANSI Std. 239-18

THIS PAGE INTENTIONALLY LEFT BLANK

Approved for public release. Distribution is unlimited.

CLUTTER-COMPENSATING ADAPTIVE WAVEFORMS WITH COGNITIVE RADAR USING ACTUAL TARGET MEASUREMENTS FOR TARGET CLASSIFICATION

Ben Muwei Bey
Major, Republic of Singapore Air Force
BEE, National University of Singapore, 2009

Submitted in partial fulfillment of the
requirements for the degree of

MASTER OF SCIENCE IN ELECTRICAL ENGINEERING

from the

NAVAL POSTGRADUATE SCHOOL
September 2019

Approved by: Ric Romero
Advisor

David C. Jenn
Second Reader

Douglas J. Fouts
Chair, Department of Electrical and Computer Engineering

THIS PAGE INTENTIONALLY LEFT BLANK

ABSTRACT

In this work, we investigate the target classification performance of a cognitive radar (CRr) using EM-simulated ground-based target responses and EM-measured aerial target responses in the presence of transmit waveform-dependent clutter. Moreover, we consider a more realistic target classification scenario where the cognitive radar is pointing at a look angle of 30°, in which clutter can definitely be a major interference. Previous works included EM-simulated target responses with an adaptive waveform design technique known as probability-weighted energy (PWE) for target recognition; however, practically measured power spectrum density (PSD) for signal-dependent clutter was not considered. Therefore, it is essential to build on prior works by considering signal-dependent clutter using measured target responses and a practical clutter model. We design clutter-compensating adaptive waveforms for CRr to improve classification in the presence of both narrowband and wideband clutter. Our results show improvement in classification performance of clutter-mitigating SNR and MI-based waveforms used in conjunction with PWE.

THIS PAGE INTENTIONALLY LEFT BLANK

Table of Contents

List of Figures

THIS PAGE INTENTIONALLY LEFT BLANK

List of Tables

THIS PAGE INTENTIONALLY LEFT BLANK

List of Acronyms and Abbreviations

AWGN	additive white Gaussian noise
CRr	cognitive radar
CST	computer simulation technology
CNR	clutter-to-noise power ratio
dB	decibel
DFT	discrete Fourier transform
ESD	energy spectral density
EM	electromagnetic
MAP	maximum a posteriori
MI	mutual information
MI-CC-PWE	MI-based waveform with clutter compensation using probability-weighted energy
MHT	multiple hypothesis testing
PFA	probability of false alarm
PSD	power spectral density
PWE	probability-weighted energy
PRI	pulse repetition interval
PW	pulse width
RCS	radar cross section
SNR	signal-to-noise power ratio

SINR signal-to-interference-plus-noise power ratio

SINR-CC-PWE SINR-based waveform with clutter compensation using probability-weighted energy

TNR target-to-noise power ratio

UAV unmanned aerial vehicle

VSG vector signal generator

VSA vector signal analyzer

WI wideband pulsed waveform

Acknowledgments

I would like to thank my thesis advisor, Professor Romero, for providing me the guidance required for this work. Without his patience and time in imparting the knowledge to me, this thesis would not have been possible. Special thanks to my thesis second reader, Professor David C. Jenn, as I benefited from his wealth of experience in the course of writing this thesis.

I would also like to dedicate this thesis to my wife, Eve Lim, for her self-sacrifices, and to my three children, Clara, Charmaine, and Cherlyn, for their motivation during the course of this work.

THIS PAGE INTENTIONALLY LEFT BLANK

CHAPTER 1:
Introduction

Cognitive Radar (CRr) is proposed as an intelligent signal processing sensor that learns and adapts through the interaction between the radar system and the electromagnetic (EM) environment [1]. According to the study, in CRr, the receiver gets feedback from the electromagnetic (EM) environment and forwards the learned knowledge to the transmitter. The performance of a closed-loop radar system depends on the feedback of the EM environment and the design of the transmit waveform. In [2], Bell used information theory and proposed two waveform designs for the extended radar target model. First, the waveform design is based on a deterministic target impulse response, where an optimum transmit waveform/receiver filter pair is designed to maximize the signal-to-noise ratio (SNR). This leads to a "transmit eigen-waveform solution" [2]. Second, the waveform is designed for a random target impulse response that maximizes the "mutual information (MI) between the Gaussian-distributed target ensemble with known spectral variance and the received signal in additive white Gaussian noise (AWGN)" [2]. In [3], both waveforms were adaptively modified during transmission with CRr for target classification.

In [4]-[6], the target classification performance using adaptive waveforms with signal-dependent interference was discussed and presented based on arbitrary clutter model and arbitrary target impulse responses. In recent works, EM-simulated target responses were generated using Computer Simulation Technology (CST) Microwave Studio to be used in a CRr for target recognition [7]. However, there are three practical issues not considered. First, clutter is usually the major interference instead of thermal noise (e.g., radars looking for targets on the ground). Second, EM-simulated RCS responses were not generated based on a proper grazing angle for realistic ground returns. Third, instead of using CST, truly measured target responses in an anechoic chamber were not considered. To this end, this work is to enhance realism of CRr technology in the presence of signal-dependent clutter.

1.1 Objective

The contribution of this work is the design of signal-to-interference-plus-noise ratio (SINR) and MI waveforms specifically employed using EM-measured target responses and to mitigate clutter using practical model in the received signal within the CRr framework. The signal model is shown in Figure 1.1. "The received signal is the convolution of the transmit waveform with target and clutter, hence signal-dependent interference" [5]. Two types of target responses are utilized to evaluate the performances, namely using EM-simulated ground-based target responses generated by CST simulation tool and aerial target responses measured in an anechoic chamber. In this work, we also consider target responses at a proper grazing angle where realistic ground returns could potentially limit the performance of CRr. We generate four ground target responses using the CST simulation tool where the CAD models are modified to actual size to ensure practicality. To further enhance potential and practical application, physical aerial targets are used in an anechoic chamber. The setup for the experiment consists of a vector signal generator (VSG) with a transmit antenna and a vector signal analyzer (VSA) with an antenna to collect the target response measurements. Three aerial targets are used to generate four target responses at different angles. In our closed-loop CRr simulations, we consider clutter-limited scenarios with the use of both narrowband and wideband clutter power spectral densities (PSD). Our goal is to show viability of CRr technology for both commercial and military systems where applications are clutter-limited instead of receiver noise-limited.

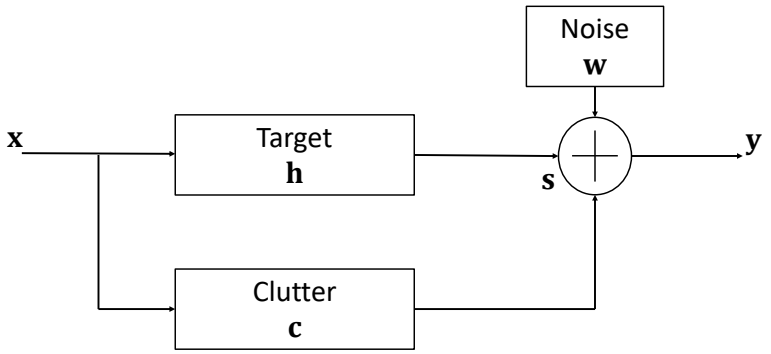

Figure 1.1. Signal model with target response in additive white Guassian noise and clutter. Adapted from [5].

1.2 Thesis Organization

This thesis is organized as follows. The signal model for the signal-dependent interference with AWGN case is covered in Chapter 2. The closed-loop radar framework for target classification, and the SINR-based and MI-based adaptive waveforms for clutter compensation are discussed in Chapter 2. The adaptive waveform design for target classification using probability-weighted energy (PWE) is discussed in Chapter 3. The target sets of ground-based target responses and aerial target responses at different angles are also discussed in Chapter 3. The use of clutter PSD is also described in Chapter 3. The results in terms of percentage or probability of classification (P_{cd}) are covered in Chapter 4. The results are obtained via Monte Carlo simulations and 10,000 trials are performed to generate P_{cd} against transmit energy. In addition, clutter-to-noise ratio (CNR) and target-to-noise ratio (TNR) are varied to obtain the target classification performance. Finally, conclusion and recommendations for future work are presented in Chapter 5.

THIS PAGE INTENTIONALLY LEFT BLANK

CHAPTER 2:
Signal Models with Signal-Dependent Interference — Clutter

The signal model with the inclusion of signal-dependent interference is shown in Figure 2.1 [4], and the closed-loop radar system is first introduced in [3]. The sampling time is normalized as in most signal processing applications. Let $x[n]$ be the transmit waveform with a vector length of L_x. Let $X[f]$ be the discrete Fourier transform of $x[n]$ where $f = 0, 1/L_x, 2/L_x, ..., 1 - 1/L_x$ [5]. Let $h[n]$ be a deterministic target and its discrete Fourier transform is $H[f]$ [7]. Let $\mathbf{c}[n]$ be a complex-valued stochastic clutter with PSD, $S_{cc}[f]$ [7]. In this formulation, clutter process does not have to be Gaussian; but in this work, we assume the interference to be a highly correlated normal process. Let $\mathbf{w}[n]$ be an AWGN from the CRr receiver with PSD, $S_{nn}[f]$. Let $\mathbf{s}[n]$ be the "convolution of the transmit waveform with both target and clutter response" (i.e., $\mathbf{s}[n] = x[n] * (h[n] + \mathbf{c}[n])$) [5]. In other words, unlike in [7] where the signal return is modeled deterministically, the echo here becomes random due to the stochastic nature of the clutter. The clutter response is spectrally shaped by the transmit waveform unlike in the classical case when the target is considered a point target. Hence, the received signal vector is $\mathbf{y}[n] = \mathbf{s}[n] + \mathbf{w}[n]$ [7].

Both deterministic and stochastic extended targets using SNR and MI matched waveforms were presented and addressed in [5], [6]. In this work, the matched waveform with signal-dependent interference, such as SINR-based waveform for clutter compensation or MI-based waveform for clutter compensation, is employed as the transmit waveform to improve radar system performance under deterministic target scenarios. In addition, other waveforms such as wideband pulsed waveform (WI), SNR-based probability-weighted energy waveform (SNR-PWE) without clutter compensation, and MI-based probability-weighted energy waveform (MI-PWE) without clutter compensation are included for target classification performance comparison.

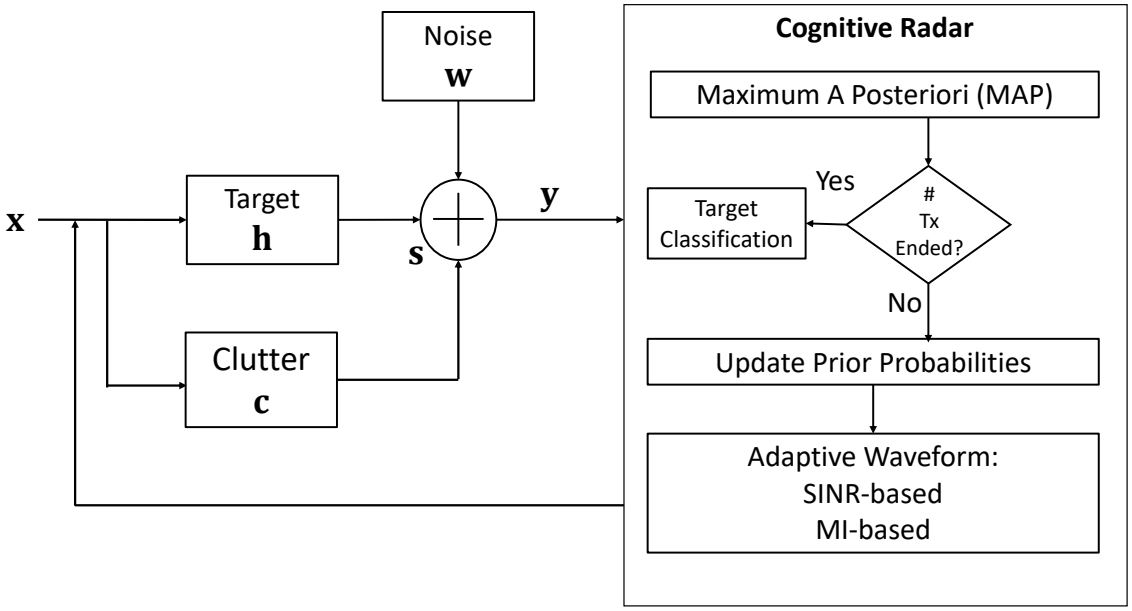

Figure 2.1. Signal model with clutter and the CRr closed-loop system. Adapted from [5].

2.1 SINR-based Waveform for Clutter Compensation

The SINR-based waveform design with clutter compensation has a frequency-domain expression that maximizes SINR. In the case of a deterministic target, the SINR-based waveform for a known target in signal-dependent interference is given by [5], [6] as

$$\text{SINR} = \sum_{f} \frac{|H[f]|^2 |X[f]|^2}{S_{cc}[f]|X[f]|^2 + S_{nn}[f]} \Delta f, \tag{2.1}$$

where $\Delta f = 1/L_x$. Notice the clutter-waveform spectrum in the denominator.

The optimum waveform that maximizes SINR in Equation (2.1) with respect to $|X[f]|^2$ is described by the waveform energy spectral density (ESD) which is given by

$$|X[f]|^2 = \max\Big[0, B(f)(A - D(f))\Big], \tag{2.2}$$

where $B(f)$ and $D(f)$ are

$$B(f) = \frac{\sqrt{|H[f]|^2 S_{nn}[f]}}{S_{cc}[f]} \tag{2.3}$$

and

$$D(f) = \sqrt{\frac{S_{nn}[f]}{|H[f]|^2}}, \tag{2.4}$$

respectively. In Equation (2.2), the energy constraint E_x determines the constant A and $|H[f]|^2$ is the ESD of the known target of length L [5]. The energy constraint with error tolerance ϵ is given by [5], [6] as

$$E_x - \frac{\epsilon}{2} \leq \sum_{f} \max\Big[0, B(f)(A - D(f))\Big] \Delta f \leq E_x + \frac{\epsilon}{2}. \tag{2.5}$$

When A is found in Equation (2.2) for a given E_x, the SINR is calculated using Equation (2.1) [5], [6].

2.2 MI-based Waveform for Clutter Compensation

The MI-based waveform design with clutter compensation is used to maximize the mutual information as described by [6]. The MI waveform design in signal-dependent interference is given by [5], [6] as

$$\mathrm{MI} = \sum_{f} \ln\left[1 + \frac{|X[f]|^2 |H[f]|^2}{S_{nn}[f] + |X[f]|^2 S_{cc}[f]}\right]\Delta f. \tag{2.6}$$

The optimum waveform in terms of MI is described by the ESD $|X[f]|^2$ via the waterfilling waveform and is given by [5], [6] as

$$|X[f]|^2 = \max\Big[0, B(f)(A - D(f))\Big], \tag{2.7}$$

where

$$B(f) = \frac{|H[f]|^2}{2S_{cc}[f] + |H[f]|^2} \tag{2.8}$$

and

$$D(f) = \frac{S_{nn}[f]}{|H[f]|^2}. \tag{2.9}$$

Once $|X[f]|^2$ is determined in Equation (2.7), the MI can be obtained from Equation (2.6). Similarly, the energy of the waveform determines the constant A [5], [6].

2.3 SINR and MI Waveform for Clutter Compensation

As described in [5], SINR and MI-based waveforms for clutter compensation or in signal-dependent interference are re-formed to mitigate clutter where the solutions allow the waveforms to avoid strong clutter energy and focus on weak clutter energy. In addition, for low-energy constraint, SINR-based waveform occupies the frequency band with higher target energy while MI-based waveform distributes its energy to occupy more frequency bands [5]. When the energy constraint starts to increase, both SINR and MI-based waveforms start to place more energy at frequency bands where clutter energy is slightly stronger [5]. This phenomenon is illustrated in Figure 2.2 [5].

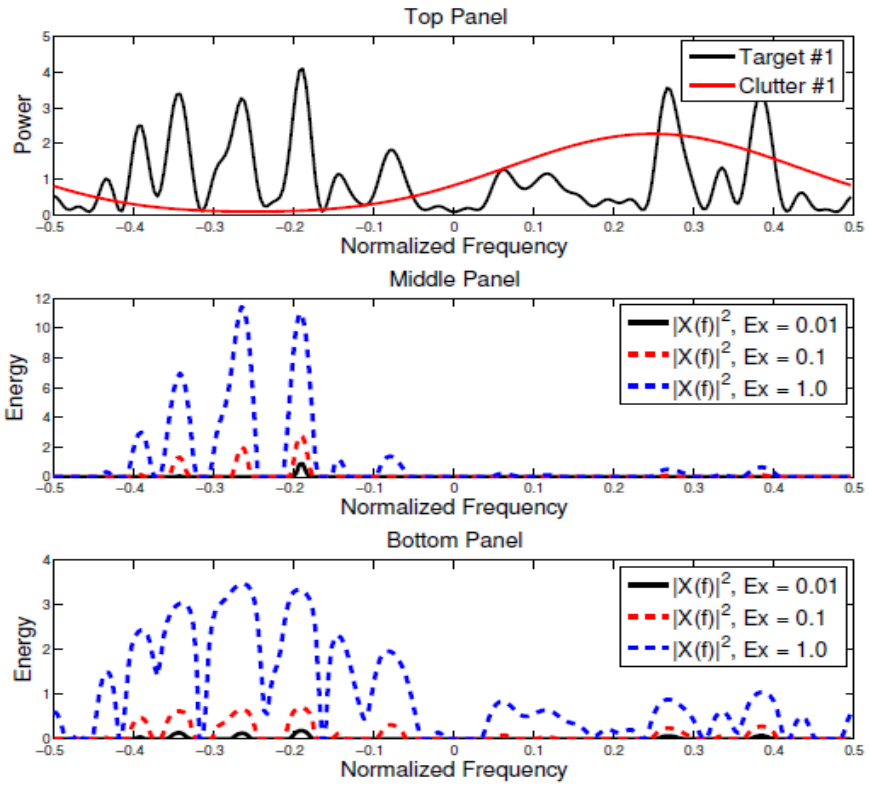

Figure 2.2. SINR and MI waveform for clutter compensation: target and clutter PSD (top panel); SINR-based waveform ESD (middle panel); and MI-based waveform ESD (bottom panel). Source: [5].

2.4 Chapter Summary

A description of the complex-valued signal model with the inclusion of signal-dependent interference such as clutter and the closed-loop radar system were introduced. The equations of SINR and MI waveforms in signal-dependent interference for deterministic targets were presented where transmit waveforms were optimized for SINR and MI. SINR and MI-based waveforms for clutter compensation were presented where the transmit waveforms avoided strong clutter and focused transmit energy on weak clutter.

CHAPTER 3:
Cognitive Radar for Target Classification in Clutter

CRr for target classification using arbitrarily generated deterministic targets was proposed in [3]. In this work, we extend the CRr by using EM-simulated ground-based targets which are more realistic just like those used in [7], [8]. However, the simulated responses in [7] had zero grazing angle and thus are not suitable when considering ground clutter. Here, we use simulated target responses that are generated from Computer Simulation Technology (CST) simulation software at a grazing angle of 30°. To bring this work closer to practical reality, aerial targets are placed in an anechoic chamber for measurements with the use of a VSG for transmission and a VSA for reception. Three small unmanned aerial vehicles (UAV) are used as targets to generate four responses at different angles.

Looking at Figure 2.1, let us consider the targets to be ground-based or aerial targets flying at low level. Both ground and target are illuminated where the CRr needs to classify one of the deterministic targets. Consequently, this multiple hypothesis testing (MHT) problem needs to be solved. Let $\mathcal{H}_1, \mathcal{H}_2, ..., \mathcal{H}_M$ be the target hypotheses with corresponding prior probabilities $P_1, P_2, ..., P_M$. The i^{th} hypothesis is given in [5] as

$$\mathcal{H}_i : \mathbf{y} = \mathbf{s}_i + \mathbf{w} = (\mathbf{h}_i + \mathbf{c}) * \mathbf{x} + \mathbf{w}, \tag{3.1}$$

where $\mathbf{h}_i$ is the i^{th} target impulse response $i = 1, 2, ..., M$, $\mathbf{c}$ is the random interference dictated by the clutter PSD, and $\mathbf{w}$ is the receiver AWGN. The AWGN is given as $\mathbf{w} \sim \mathcal{CN}(0, \sigma^2\mathbf{I})$, where σ^2 is the noise sample variance and $\mathbf{I}$ is the identity matrix. However, the clutter is correlated and transmit-signal dependence as evident in Equation (3.1). Under a given hypothesis, the joint probability density function (pdf) of the measurement is described in [5] as

$$p(\mathbf{y}_1, ..., \mathbf{y}_K) = \frac{|\mathbf{Q}^{-1}|}{|\mathbf{K_c}|\pi^{LK}|\mathbf{K_N}|^K} \exp\left[- \sum_{k=1}^{K} [\mathbf{y}]^H \mathbf{K_N}^{-1} \mathbf{y} \right] \tag{3.2}$$

$$\times \exp\left[\left[\textstyle\sum_{k=1}^{K} \mathbf{X}_k{}^H \mathbf{K_N}^{-1} \mathbf{y} \right]^H \mathbf{Q}^{-1} \textstyle\sum_{k=1}^{K} \mathbf{X}_k{}^H \mathbf{K_N}^{-1} \mathbf{y} \right],$$

where

$$\mathbf{y} = \mathbf{y}_k - \mathbf{X}_k\mathbf{h} \tag{3.3}$$

and

$$\mathbf{Q} = {\mathbf{K_c}}^{-1} + \sum_{k=1}^{K} {\mathbf{X}_k}^H {\mathbf{K_N}}^{-1}\mathbf{X}_k. \tag{3.4}$$

$\mathbf{X}_k$ is the transmit signal matrix. $\mathbf{K_c}$ and $\mathbf{K_N}$ are the clutter and noise covariance matrices, respectively. The current number of transmissions is denoted by the subscript k.

To form the adaptive transmit waveform, we first generate the unit-energy SINR and MI waveforms for each target hypothesis $\mathbf{q}_{i,\max}$. The resulting hypotheses probabilities using PWE are used to adjust and form the adaptive waveform. To form the PWE waveform, each target optimized waveform is scaled by the updated probability and is given by [8] as

$$\mathbf{x}_{\text{pwe}} = \sum_{i=1}^{M} \sqrt{P_i}\mathbf{q}_{i,\max}, \tag{3.5}$$

and transmit energy constraint is ensured by

$$\mathbf{x} = \sqrt{E_x}\frac{\mathbf{x}_{\text{pwe}}}{\sqrt{E_{x_{\text{pwe}}}}}, \tag{3.6}$$

where $E_{x_{\text{pwe}}}$ is the energy of $\mathbf{x}_{\text{pwe}}$ which is defined in Equation (3.5). The Bayes' probability update rule, for the i^{th} target at $(k+1)^{\text{th}}$ iteration, is used as part of the CRr to retain knowledge from the previous received signals. It is given by [5], [8] as

$$P_i^{(k+1)} = \beta p(\mathbf{y}^{(k+1)}|\mathcal{H}_i)P_i^{(k)}, \tag{3.7}$$

where the superscript denotes the iteration number, and $p(\mathbf{y}^{(k)}|\mathcal{H}_i)$ is the pdf after the k^{th} iteration. In addition, a total probability of one for each iteration is ensured by β. "Based on the most probable hypothesis after the last waveform is transmitted, maximum a posteriori (MAP) is used to determine the target decision" [3], [8].

3.1 Clutter Power Spectrum Modelling

In [10], road clutter spectrum was reported based on FMCW radar operating at 24 GHz that was equipped in a moving vehicle. The study also presented the theoretical and practical clutter spectrum results for comparison. The Doppler clutter power spectrum of a vehicle (equipped with radar) moving towards or away from a clutter cell depends on vehicle relative direction and the clutter area. The received echoes can have random phases, amplitudes, and angles of arrival. The Doppler shift frequency is given by

$$f_d = f_m \cos\theta \cos\phi \tag{3.8}$$

where the maximum Doppler frequency f_m is given by $\frac{2V}{\lambda}$. The speed of the vehicle is V and λ is the wavelength corresponding to the carrier frequency. The experimental results of measuring a stationary clutter in a park are shown in Figure 3.1, where the static clutter is focused mostly between 0 to 200 Hz [10].

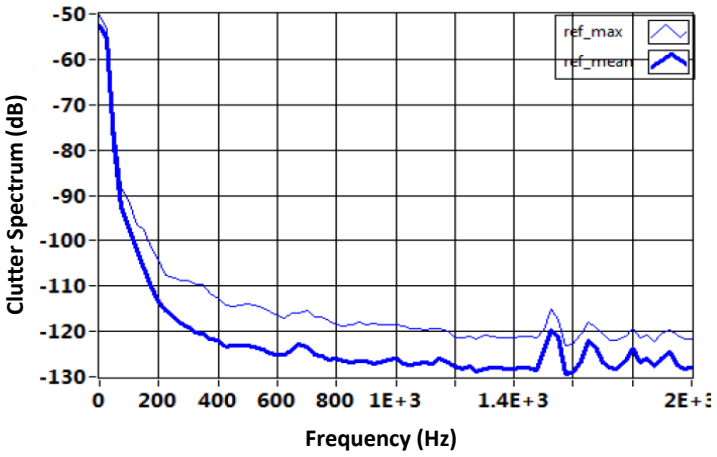

Figure 3.1. PSD of measured clutter. Source: [10].

In [11], clutter spectrum from trees at X-band showed that Gaussian-shaped spectrum is not a better curve fit as compared to power law-shaped spectrum since Guassian curve fit rolled off too quickly. According to the study, this pheonomenon was discovered by Fishbein, et al, who attempted to generate models of clutter spectrum from trees at X-band. Both the clutter PSD of a Guassian and power law curves are shown in Figure 3.2. The clutter power spectrum of a power law curve is described in [11] in the form

$$S_{cc}(f) = \sigma_{DC}\left(\frac{1}{1 + (\frac{f}{f_c})^n}\right), \tag{3.9}$$

where σ_{DC} denotes the power return for the clutter. The cutoff frequency is denoted by f_c, and integer n is chosen for best fit. Making use of Equation (3.9), we construct a similar power law curve to represent the clutter model for this work. The plot is generated based on a platform traveling at 20 m/s, and transmitting at 2.5 GHz with aspect angles of 30° in elevation ($\theta_{el} = 30°$) and 165° in azimuth ($\theta_{az} = 165°$). With f from 0 to 120 MHz, the approximated power law curve is plotted as shown in Figure 3.3.

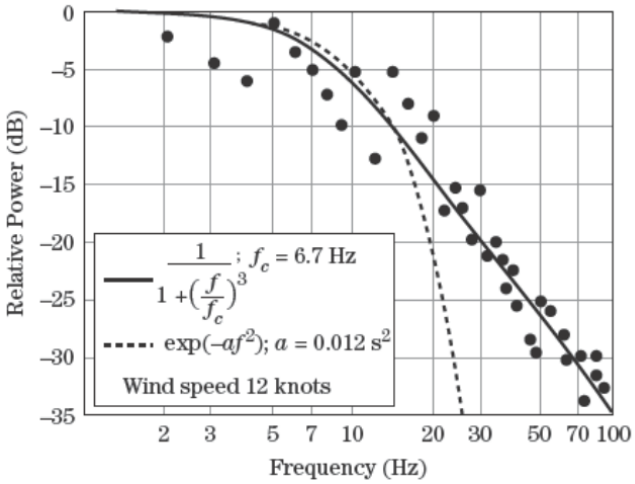

Figure 3.2. PSD of trees at X-band with Guassian and power function curve fits. Source: [11].

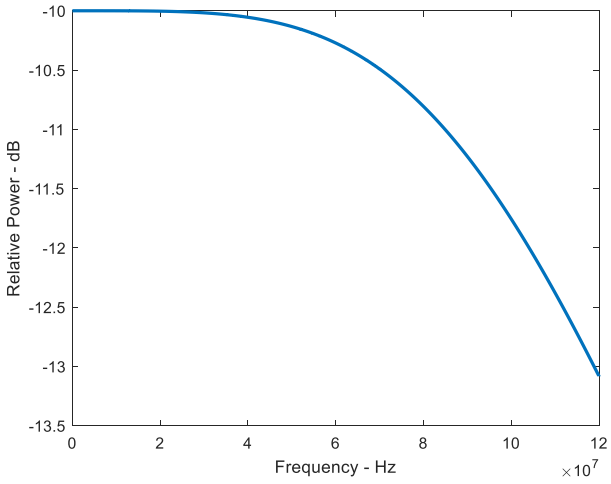

Figure 3.3. Resulting PSD of clutter from 0 to 120 MHz with carrier frequency 2.5 GHz using Equation (3.9).

3.1.1 Narrowband and Wideband Clutter Model

The clutter power spectra described in [10] and [11] provide a basis to generate generic but practical clutter PSDs in this work. To model clutter PSD, we consider both narrowband and wideband clutter where the Hamming-shaped and Blackman-Harris-shaped PSDs are used which are centered at 0 Hz as is usual in clutter scenarios. The PSDs of the narrowband and wideband clutter (normalized frequency) are designed based on a less conservative approach, where the clutter occupies the target response bandwidth of 1 GHz, and centered at 0 Hz. The PSD models for both narrowband and wideband scenarios are shown in Figure 3.4.

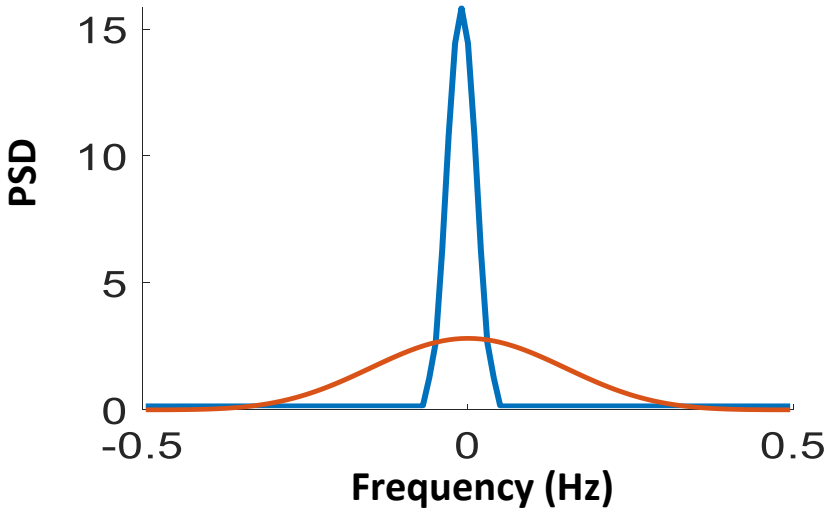

Figure 3.4. Clutter models used in simulations: PSD of wideband and narrowband clutter (normalized frequency).

3.2 CST-Generated Target RCS Responses at 30° Degree Grazing Angle

While RCS responses of high fidelity CAD target models were used in previous work [7], those targets were at 0° in elevation ($\theta_{el} = 0°$), and thus are not appropriate when ground clutter is considered. It is therefore imperative to produce ground-based target responses at proper grazing angles. The clutter-mitigating CRr presented here is applicable to both static and moving targets or platforms. For moving targets and/or platforms, the proper Doppler shift can easily be addressed by subtracting the Doppler frequency shift due to that motion.

Four ground-based target CAD models from publicly open sources are modified to actual size for practicality. CST simulation software is used to generate the ground targets RCS responses. The EM-simulated RCS frequency responses between 3 to 4 GHz (S-band radar) are generated through an asymptotic solver that utilizes the ray tracing technique. The two incidence or aspect angles are: a) azimuth of 165° ($\theta_{az} = 165°$) and elevation of 30° ($\theta_{el} = 30°$), and b) azimuth of 180° ($\theta_{az} = 180°$) and elevation of 30° ($\theta_{el} = 30°$). The ground target models and their RCS electric field (E-field) responses for 165° in azimuth ($\theta_{\text{az}} = 165°$) and 30° in elevation ($\theta_{\text{el}} = 30°$) are shown in Figure 3.5 and Figure 3.6, respectively. The ground target CAD models and their RCS E-field responses for 180° in azimuth ($\theta_{az} = 180°$) and 30° in elevation ($\theta_{el} = 30°$) are shown in Figure 3.7 and Figure 3.8, respectively.

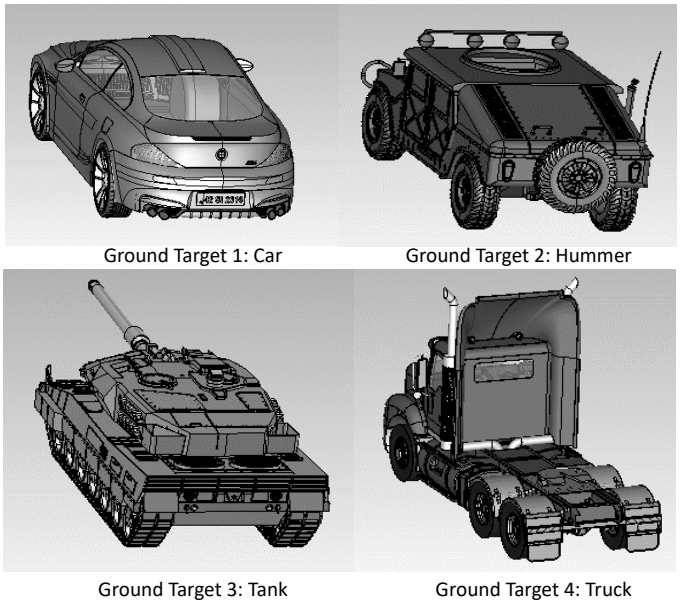

Figure 3.5. Ground-based target CAD models: car, Hummer, tank and truck. Aspect angle of 165° in azimuth ($\theta_{az} = 165°$) and 30° in elevation ($\theta_{el} = 30°$).

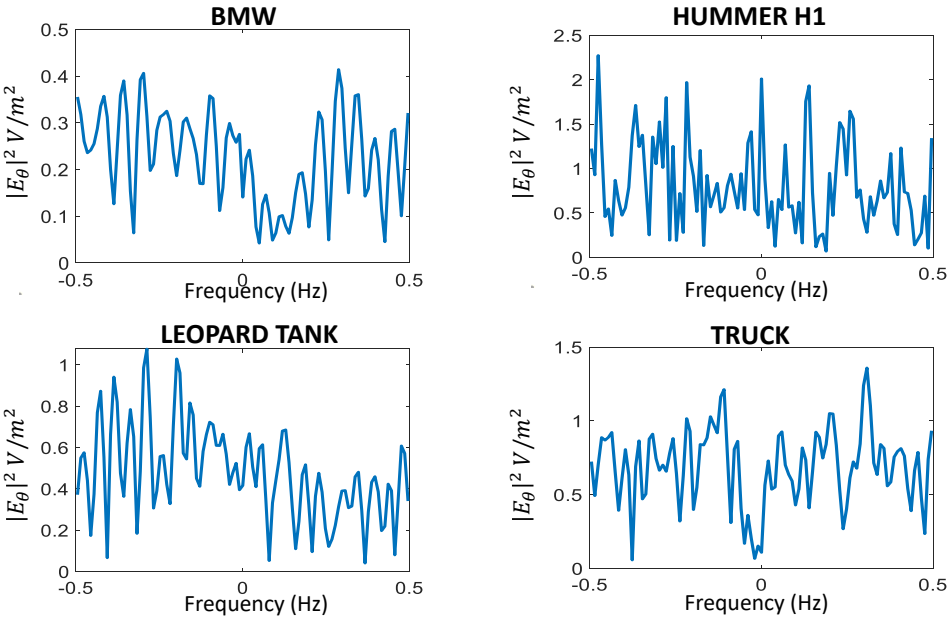

Figure 3.6. Ground-based RCS targets' 3 to 4 GHz frequency responses at $\theta_{az} = 165°$ and $\theta_{el} = 30°$ shown in normalized frequency.

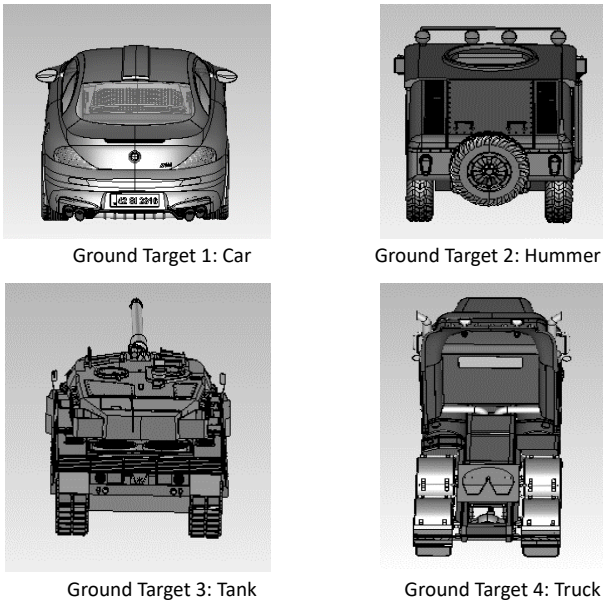

Figure 3.7. Ground-based targets CAD model: car, Hummer, tank and truck. Aspect angle of 180° in azimuth ($\theta_{az} = 180°$) and 30° in elevation ($\theta_{el} = 30°$).

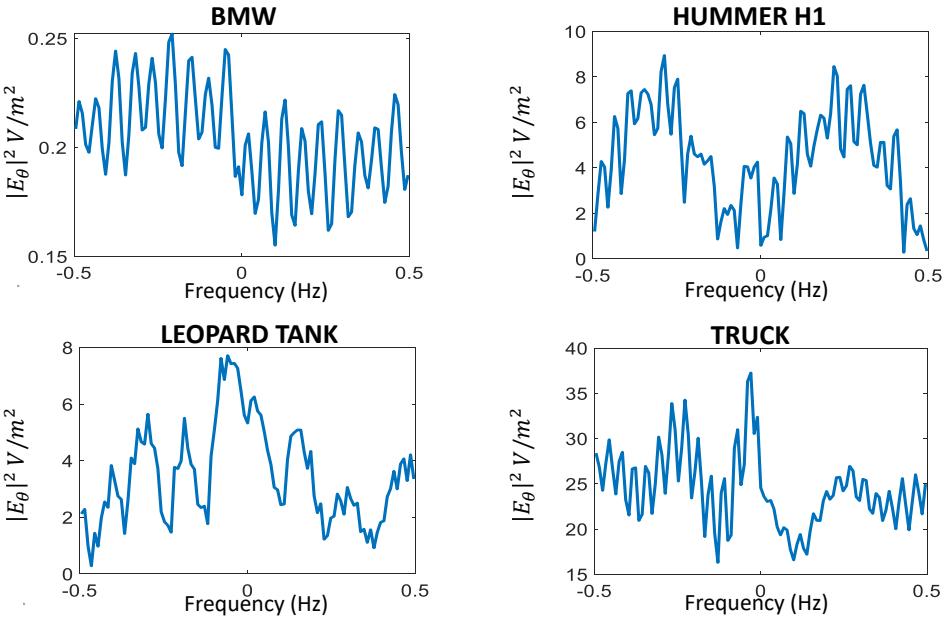

Figure 3.8. Ground-based RCS targets' 3 to 4 GHz frequency responses at $\theta_{az} = 180°$ and $\theta_{el} = 30°$ shown in normalized frequency.

3.3 Target Impulse Response Measurements in the Anechoic Chamber

Three small aerial targets are used to measure their impulse responses in a radio-frequency (RF) anechoic chamber. The measured impulse responses are easily converted to frequency responses via traditional Fourier methods. A RF anechoic chamber has the benefits of preventing surrounding EM waves from entering the receiving antenna with minimal to no reflected signal from walls during measurement. The setup in the RF anechoic chamber requires the VSG, VSA and antennas. The VSG transmits 2000 pulses via a carrier at a pulse width (PW) of 10 ns and pulse repetition interval (PRI) of 200 ns. We desire 1 GHz bandwidth in the 2-3 GHz carrier band but the VSA instantaneous bandwidth is limited to 120 MHz. Thus, the series of pulses are repeated from 2 to 3 GHz in 100 MHz increments. The VSA collects the 2000 received signals for post-processing through MATLAB. The VSG (used as transmitter) and the VSA (used as receiver) are shown in Figure 3.9. Coherent integration is used to obtain higher SNR. The targets and equipment setup in the anchoic chamber are shown in Figure 3.10. The two incidence or aspect angles are: a) RiteWing - The Zephyr II, DJI M100 and Quadcopter-MosquitoHawk at 30° in azimuth ($\theta_{az} = 30°$) and 30° in elevation ($\theta_{el} = 30°$), and b) only RiteWing - The Zephyr II at 0° in azimuth ($\theta_{az} = 0°$) and 30° in elevation ($\theta_{el} = 30°$). Through pulse integration and post-processing via MATLAB, the magnitude frequency responses are generated. The aerial target models are shown in Figure 3.11 and the four target responses are shown in Figure 3.12.

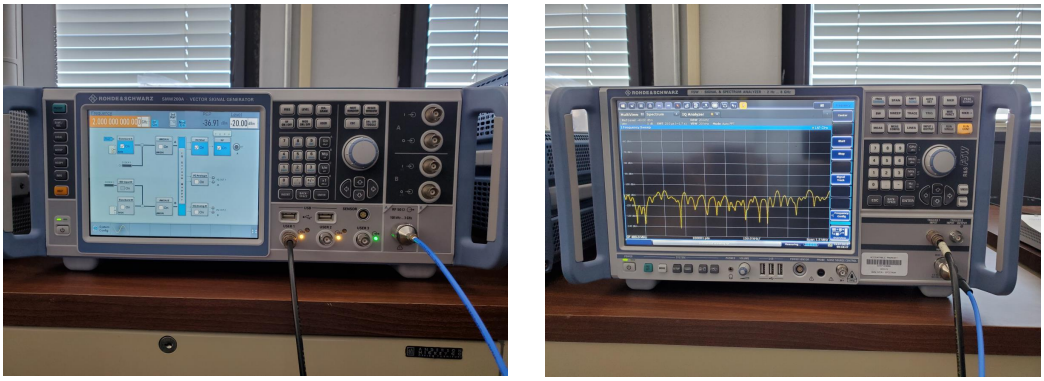

Figure 3.9. Transmitter and receiver for target impulse response measurement.

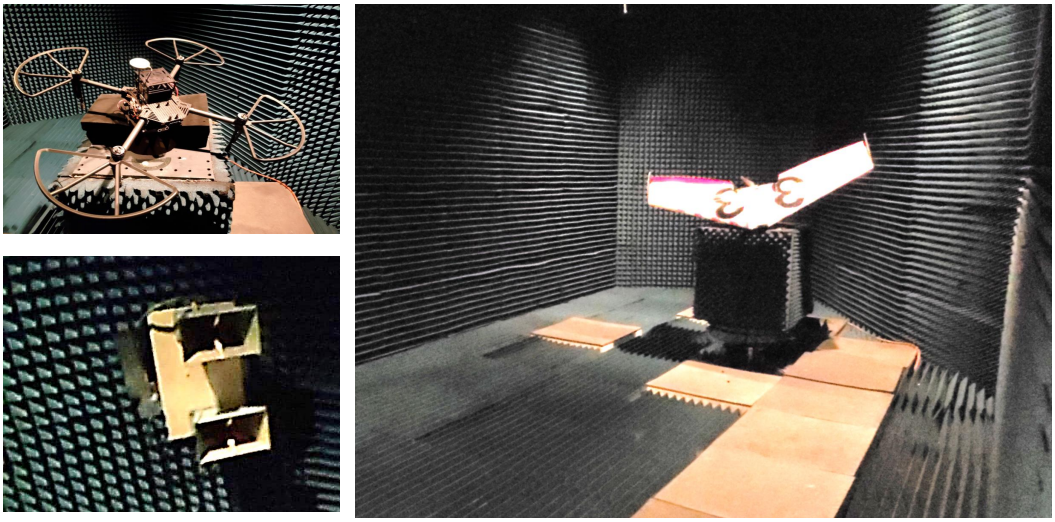

Figure 3.10. Antennas and radar targets (airplane and drones) in anechoic chamber.

Figure 3.11. Airplane and drones used for impulse response measurement.

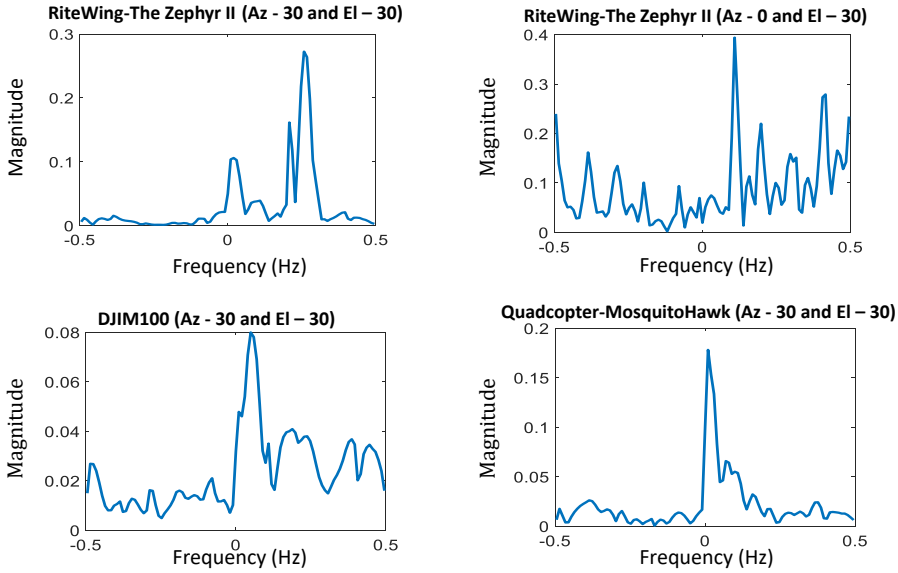

Figure 3.12. Aerial targets' 2-3 GHz frequency responses shown in normalized frequency (targets are placed 6 m away from antennas).

3.4 SINR-based Waveform for Clutter Compensation on Measured Target Frequency Responses

As described in Chapter 2, the SINR-based waveform design for clutter compensation has a frequency-domain expression that maximizes SINR. In the case of a deterministic target, the SINR metric can be calculated using Equation (2.1). When SINR-based waveform for clutter compensation is employed, the adaptive waveform avoids high energy clutter region and transmits only at low energy clutter regions. An example of a SINR waveform with signal-dependent interference under the influence of a Hummer target response, hence clutter compensating waveform, is shown in Figure 3.13.

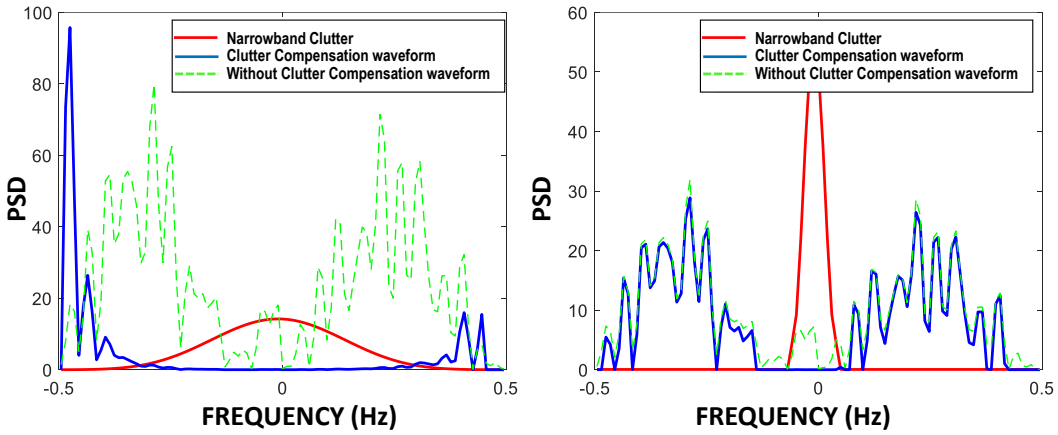

Figure 3.13. SINR waveform with clutter compensation.

3.5 MI-based Waveform for Clutter Compensation on Measured Target Frequency Responses

The MI-based waveform for clutter compensation is designed for stochastic target in clutter where it maximizes the mutual information as described by [5], [6]. The MI metric can be calculated using Equation (2.6) [5], [6]. When MI-based waveform for clutter compensation is employed, the waveform avoids the high energy clutter region and transmits at high energy target regions in the frequency domain, hence clutter compensation waveform is achieved. An example of a MI waveform with signal-dependent interference under the influence of a Hummer target frequency response is shown in Figure 3.14.

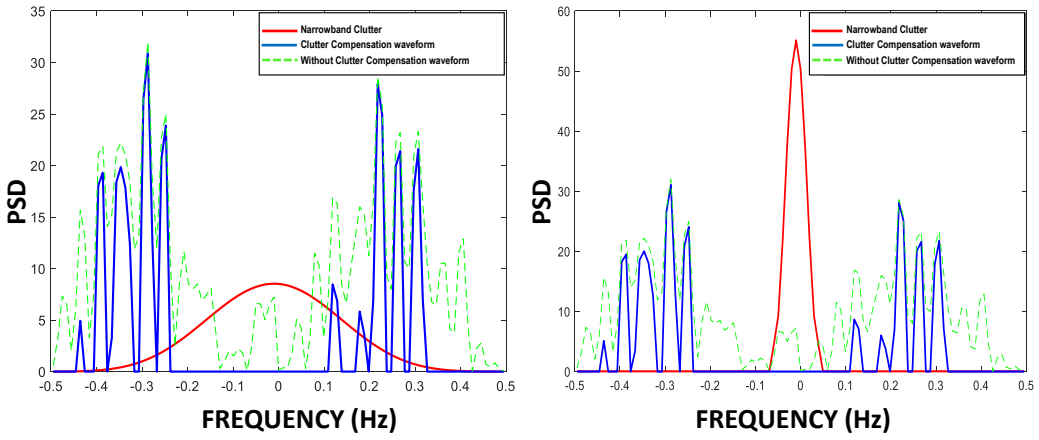

Figure 3.14. MI waveform with clutter compensation.

3.6 Chapter Summary

A stationary clutter PSD was used as a basis to generate a clutter PSD model to generate interference realizations for Monte Carlo simulations for this work. Moreover, narrowband and wideband clutter were designed to ensure a less conservative approach when included in the simulation. To generate target RCS responses at a grazing angle for realistic ground or clutter returns, the first approach used CAD target models where the CST simulation software generated the EM-simulated frequency responses. With the use of CST simulation software, two incidence angles for four targets were generated: a) 180° in azimuth (θ_{az} = 180°) and 30° in elevation (θ_{el} = 30°), and b) 165° in azimuth (θ_{az} = 165°) and 30° in elevation (θ_{el} = 30°). The second approach of generating target impulse responses was to use physical aerial targets in the RF anechoic chamber to generate more realistic target measurements. The anechoic chamber method was chosen since it could prevent unwanted EM waves from the surroundings and achieve minimal to no reflected signal from walls during measurements. Two incidence angles were used to generate the responses: a) RiteWing - The Zephyr II, DJIM100 and Quadcopter - MosquitoHawk positioned at 30° in azimuth (θ_{az} = 30°) and 30° in elevation (θ_{el} = 30°), and b) RiteWing - The Zephyr II positioned at 0° in azimuth (θ_{az} = 0°) and 30° in elevation (θ_{el} = 30°). With the target magnitude frequency responses, SINR-based and MI-based waveforms were derived to illustrate how waveforms were shaped under wideband or narrowband clutter scenarios.

THIS PAGE INTENTIONALLY LEFT BLANK

CHAPTER 4:
Results

The MAP detection rule is used to determine which target is present for one transmission, and in the case of CRr, multiple transmissions are considered. The system selects one of the possible M targets based on the highest hypothesis probability after the last transmission. Adaptive waveform performance is calculated with the percentage of correct classification (P_{cd}). To show the utility of the clutter-compensated waveforms, we will compare them to the uncompensated counterparts. The waveforms used are: a) WI, b) SNR-PWE, c) MI-PWE, d) SINR-CC-PWE, and e) MI-CC-PWE.

The two ground-based target sets and one aerial target set are used in generating P_{cd} against transmit waveform energy E_x over $10,000$ Monte Carlo simulations. Both wideband and narrowband clutter are considered for comparison. Single transmission and three transmissions are considered and the performance results are compared. Four combinations of CNR and TNR are considered for the three target sets: a) CNR at 0 dB and TNR at 13 dB, b) CNR at 3 dB and TNR at 13 dB, c) CNR at 6 dB and TNR at 20dB, and d) CNR at 10 dB and TNR at 16 dB. A total of 48 test cases are simulated to generate the percentage of correct classification (P_{cd}) to compare adaptive waveforms with clutter compensation against the other waveforms.

4.1 Target Classification Performance—Ground Target Responses for 165° in Azimuth and 30° in Elevation

Looking at Figure 4.1, we present the CRr closed loop system where four targets are positioned at 165° in azimuth and 30° in elevation. Clearly, with CRr, the waveforms for clutter compensation will be adapted before transmitting as described in Chapter 3. We show in Table 4.1 the first 16 test cases for ground target responses at 165° in azimuth ($\theta_{az} = 165°$) and 30° in elevation ($\theta_{el} = 30°$). The first 8 test cases considered are with wideband clutter for 1 transmission and 3 transmissions, whereas the next eight test cases considered are with narrowband clutter. Four different combinations of CNR and TNR are varied to obtain the adaptive waveform performance.

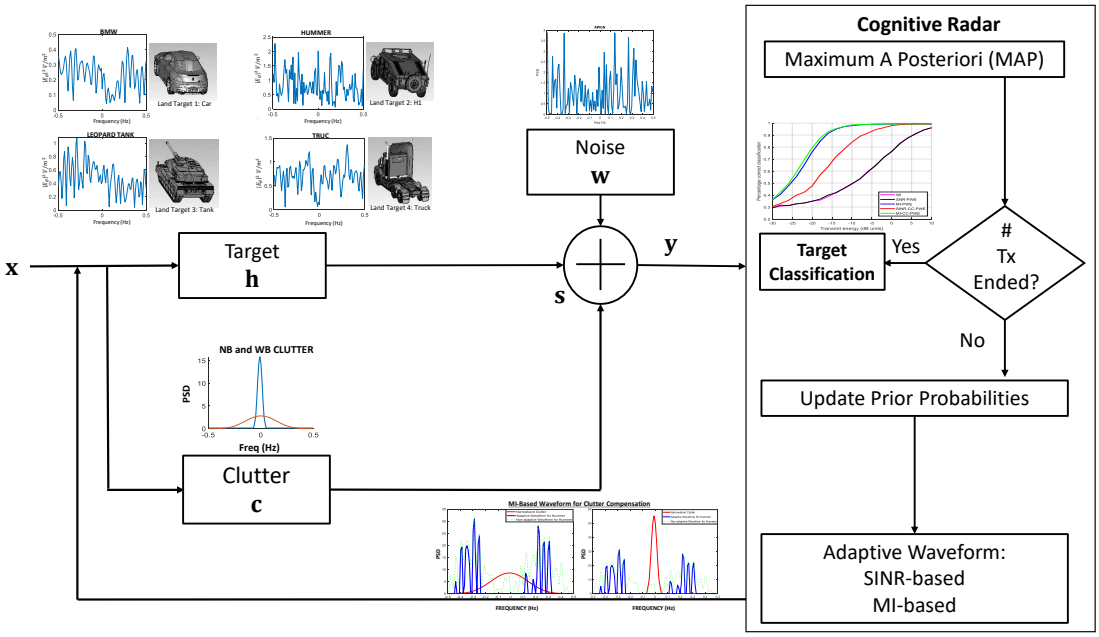

Figure 4.1. CRr closed loop diagram: ground target responses for $\theta_{az} = 165°$ and $\theta_{el} = 30°$.

Table 4.1. Test cases for ground target responses at Az = 165° and El = 30° in signal-dependent interference

Ground Target Responses at Az = 165° and El = 30°					
Test Cases	Target Responses	Clutter	CNR (dB)	TNR (dB)	# of Transmission
1	Ground Target Responses at Az = 165° and El = 30°	Wideband	0	13	1
2			3	13	1
3			6	20	1
4			10	16	1
5			0	13	3
6			3	13	3
7			6	20	3
8			10	16	3
9	Ground Target Responses at Az = 165° and El = 30°	Narrowband	0	13	1
10			3	13	1
11			6	20	1
12			10	16	1
13			0	13	3
14			3	13	3
15			6	20	3
16			10	16	3

4.1.1 Wideband Clutter—Target Classification for One and Three Transmissions

In this section, we discuss the classification performance for test cases 1 to 8. Referring to the classification performance in Figure 4.2, we observe that MI-CC-PWE, MI-PWE and SINR-CC-PWE outperform WI and SNR-PWE. The performance of MI-CC-PWE under wideband clutter is the best where it achieves the best P_{cd} at all transmit energy levels. From Figure 4.3, it can be seen that the performance improves significantly for adaptive waveforms under multiple transmissions. For instance, comparing test case 2 (in Figure 4.2 upper right hand corner subfigure) for one transmission and test case 6 (in Figure 4.3 upper right hand corner subfigure) for three transmissions, P_{cd} with MI-CC-PWE improves by approximately 0.2, (from 0.75 to 0.95) at transmit energy of -15 dB (J). This shows that with even more transmissions, the P_{cd} can be further improved; thus the radar is behaving as a CRr.

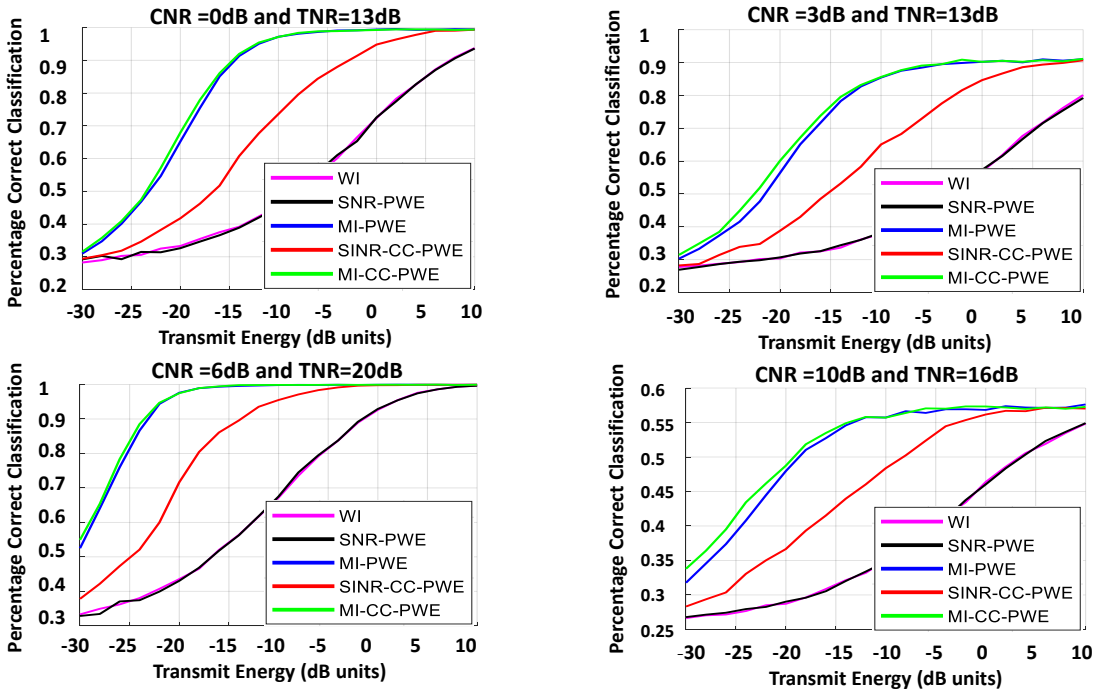

Figure 4.2. One transmission on ground target (wideband clutter)—classification performance for WI, SNR-PWE, MI-PWE, SINR-CC-PWE and MI-CC-PWE waveforms at $\theta_{az} = 165°$ and $\theta_{el} = 30°$.

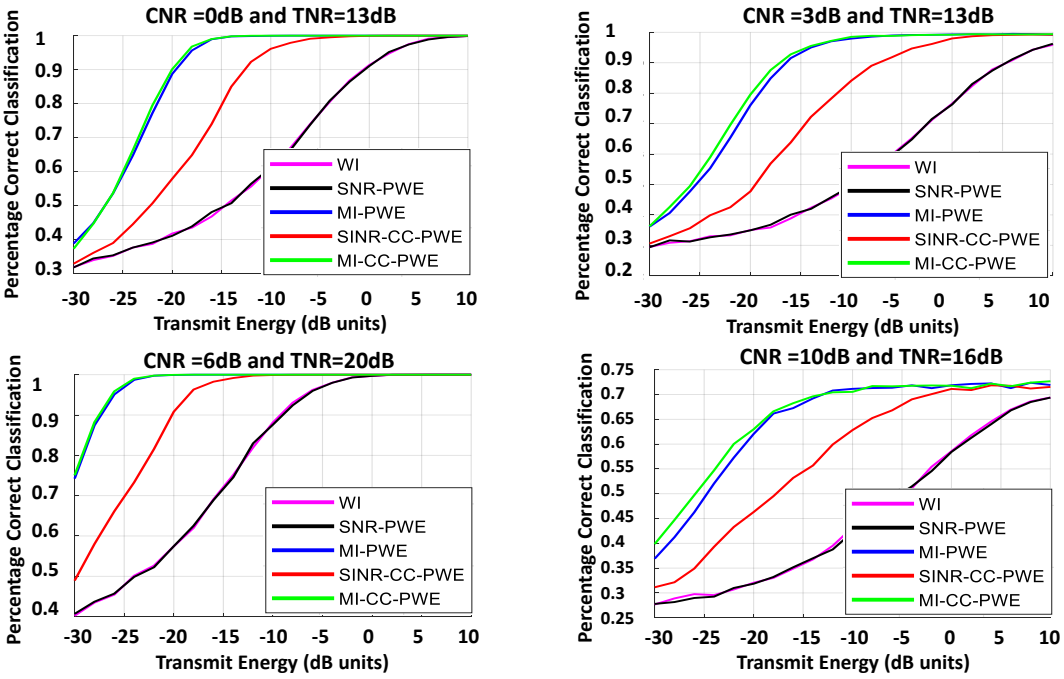

Figure 4.3. Three transmissions on ground target (wideband clutter)—classification performance for WI, SNR-PWE, MI-PWE, SINR-CC-PWE and MI-CC-PWE waveforms at $\theta_{az} = 165^{\circ}$ and $\theta_{el} = 30^{\circ}$.

4.1.2 Narrowband Clutter—Target Classification for One and Three Transmissions

In this section, we discuss the classification performance for test cases 9 to 16. As expected, the classification performance under narrowband clutter is slightly better compared to wideband clutter since less total clutter energy over the entire frequency band interacts with the target response before convolution with the transmit waveform. The performance for WI, SNR-PWE, MI-PWE, SINR-CC-PWE and MI-CC-PWE waveforms for target classification at $\theta_{az} = 165°$ and $\theta_{el} = 30°$ are shown in Figure 4.4. Similar to the first 8 test cases, MI-CC-PWE, MI-PWE and SINR-CC-PWE outperform WI and SNR-PWE. MI-CC-PWE performs the best as it achieves the best P_{cd} for all transmit energy levels. The performance using three transmissions are shown in Figure 4.5. Similar to wideband clutter test cases (1 to 8), the results show that with more transmissions, the P_{cd} increases.

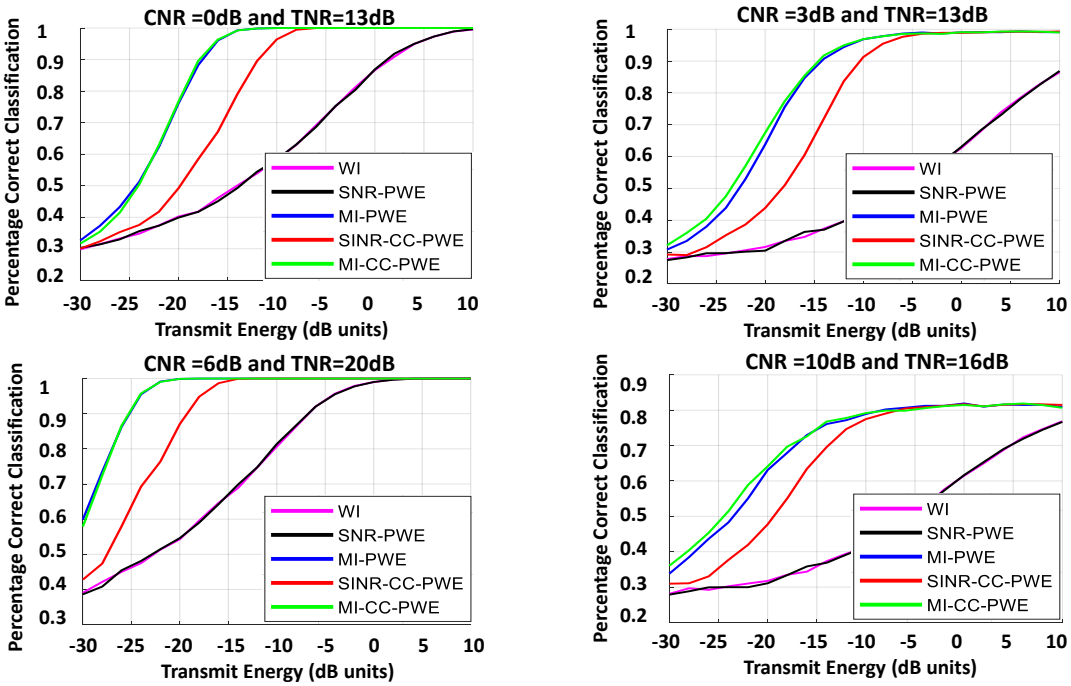

Figure 4.4. One transmission on ground target (narrowband clutter)—classification performance for WI, SNR-PWE, MI-PWE, SINR-CC-PWE and MI-CC-PWE waveforms at $\theta_{az} = 165°$ and $\theta_{el} = 30°$.

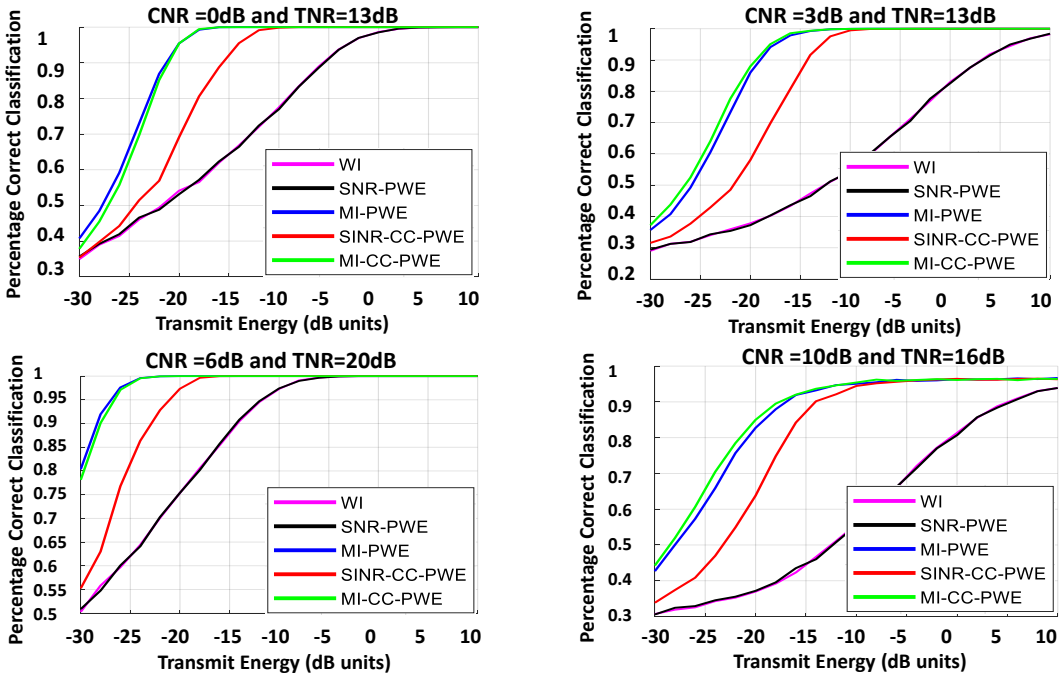

Figure 4.5. Three transmissions on ground target (narrowband clutter)—classification performance for WI, SNR-PWE, MI-PWE, SINR-CC-PWE and MI-CC-PWE waveforms at $\theta_{az} = 165°$ and $\theta_{el} = 30°$.

4.2 Target Classification Performance—Ground Target Responses for 180° in Azimuth and 30° in Elevation

In Figure 4.6, we present the CRr closed loop system where four targets are positioned at 180° in azimuth and 30° in elevation. As described in Chapter 3, the adaptive waveform for clutter compensation will be adapted according to the EM environment such as clutter or noise incorporated in the received signal. We show in Table 4.2 the next 17 to 32 test cases that are used on ground target responses for 180° in azimuth ($\theta_{az} = 180°$) and 30° in elevation ($\theta_{el} = 30°$) for both wideband and narrowband clutter with varying CNR and TNR.

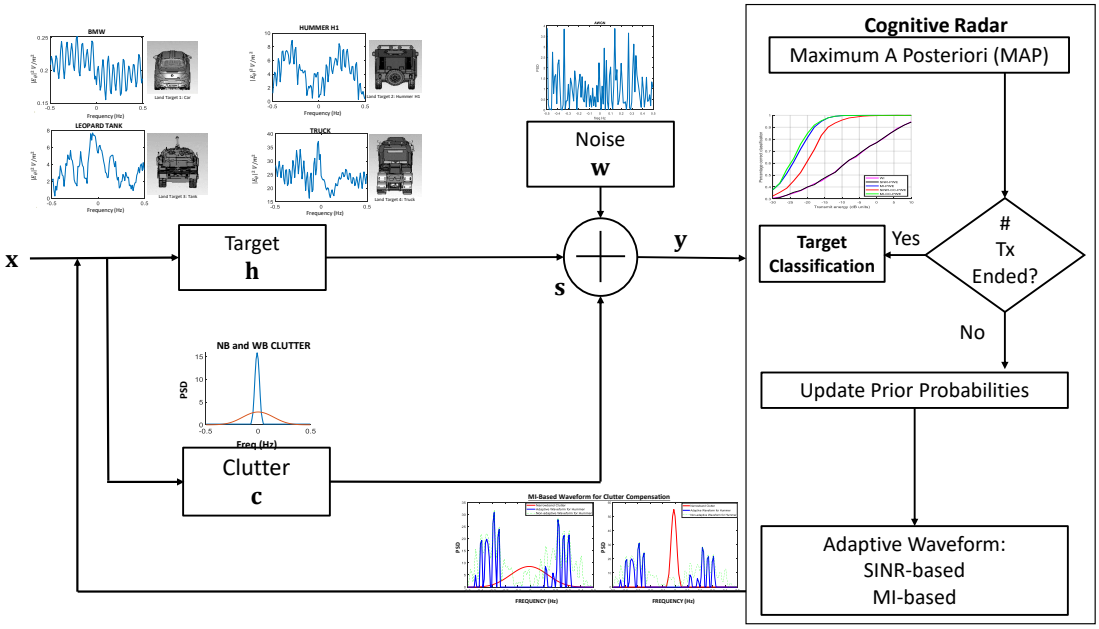

Figure 4.6. CRr closed loop diagram: ground target responses for $\theta_{az} = 180°$ and $\theta_{el} = 30°$.

Table 4.2. Test cases for ground target responses at Az = 180° and El = 30° in signal-dependent interference

Ground Target Responses at Az = 180° and El = 30°					
Test Cases	Target Responses	Clutter	CNR (dB)	TNR (dB)	# of Transmission
17	Ground Target Responses at Az = 180° and El = 30°	Wideband	0	13	1
18			3	13	1
19			6	20	1
20			10	16	1
21			0	13	3
22			3	13	3
23			6	20	3
24			10	16	3
25	Ground Target Responses at Az = 180° and El = 30°	Narrowband	0	13	1
26			3	13	1
27			6	20	1
28			10	16	1
29			0	13	3
30			3	13	3
31			6	20	3
32			10	16	3

4.2.1 Wideband Clutter—Target Classification for One and Three Transmissions

In this section, we discuss the classification performance for test cases 17 to 24. The performance for WI, SNR-PWE, MI-PWE, SINR-CC-PWE and MI-CC-PWE waveforms for target classification at $\theta_{az} = 180°$ and $\theta_{el} = 30°$ for the 4 combinations of CNR and TNR under wideband clutter are shown in Figure 4.7. The performance under three transmissions are shown in Figure 4.8. The performance results are very similar to test cases (1 to 8) where SINR-CC-PWE, MI-PWE and MI-CC-PWE outperform the WI and SNR-PWE. MI-CC-PWE performs the best as it achieves the best P_{cd} for all transmit energy levels. For the performance of three transmissions, similar results can be observed when comparing with test cases 5 to 8 (Figure 4.3), where the P_{cd} significantly improves with more transmissions for all waveforms. MI-CC-PWE performs better against the rest of the waveforms when the CNR increases.

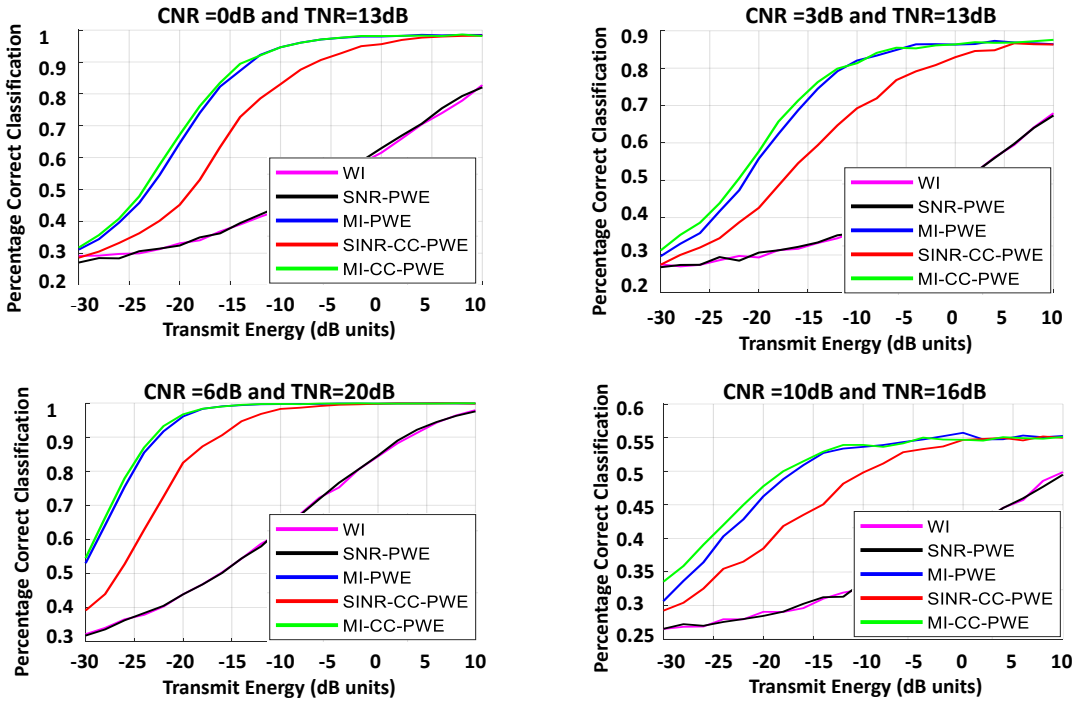

Figure 4.7. One transmission on ground target (wideband clutter)—classification performance for WI, SNR-PWE, MI-PWE, SINR-CC-PWE and MI-CC-PWE waveforms at $\theta_{az} = 180°$ and $\theta_{el} = 30°$.

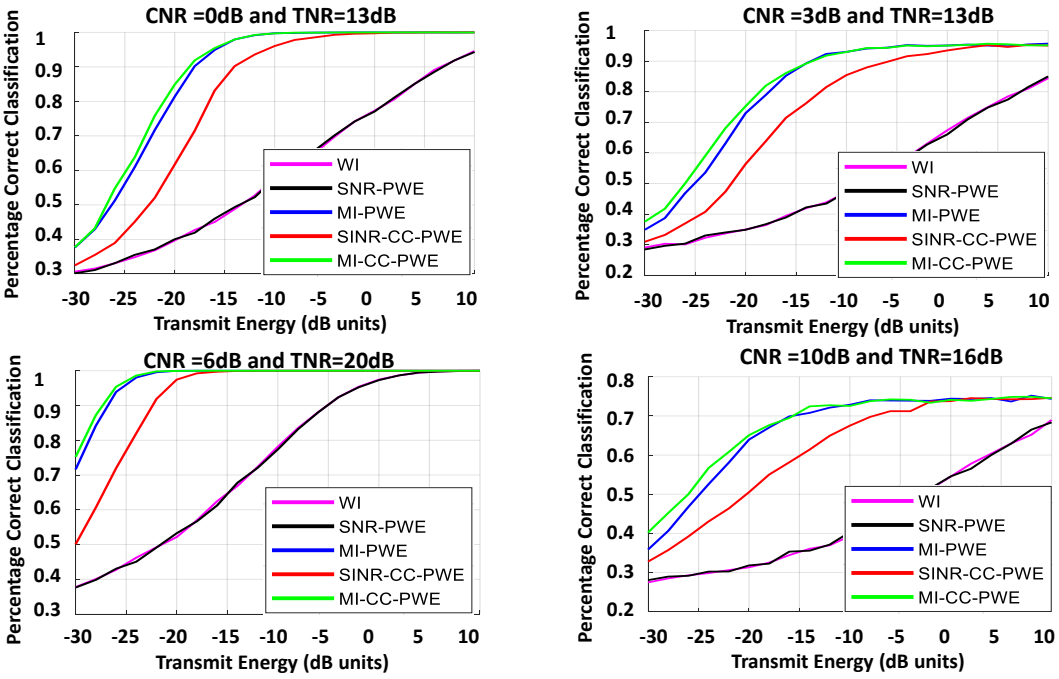

Figure 4.8. Three transmissions on ground target (wideband clutter)—classification performance for WI, SNR-PWE, MI-PWE, SINR-CC-PWE and MI-CC-PWE waveforms at $\theta_{az} = 180°$ and $\theta_{el} = 30°$.

4.2.2 Narrowband Clutter—Target Classification for One and Three Transmissions

In this section, we discuss the classification performance for test cases 25 to 32. Similar to previous result obtained for test cases (9 to 16), the classification performance under narrowband clutter is slightly better compared to wideband clutter since less total clutter energy over the entire frequency band interacts with the target response before convolution with the transmit waveform. The performance for WI, SNR-PWE, MI-PWE, SINR-CC-PWE and MI-CC-PWE waveforms for target classification at $\theta_{az} = 180°$ and $\theta_{el} = 30°$ are shown in Figure 4.9. Similar results are obtained where MI-CC-PWE, MI-PWE and SINR-CC-PWE outperform WI and SNR-PWE. Also, MI-CC-PWE performs the best. The performance using three transmissions are shown in Figure 4.10. Comparing with test cases 13 to 16 (Figure 4.5) under 3 transmissions, we obtain similar performance where the P_{cd} increases with more transmissions.

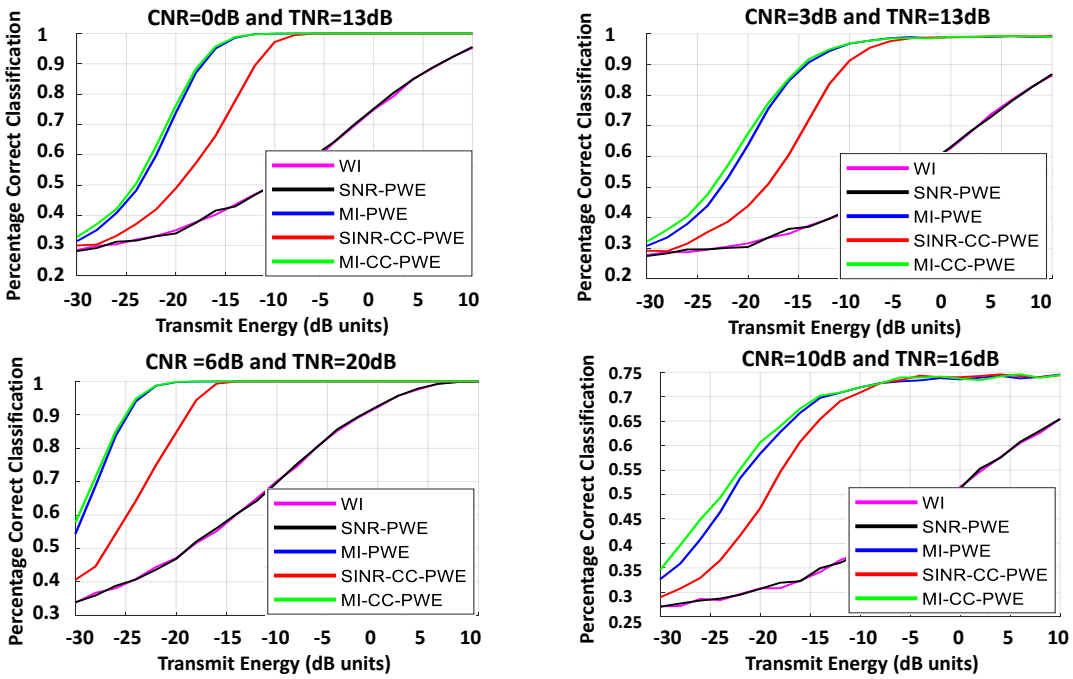

Figure 4.9. One transmission on ground target (narrowband clutter)—classification performance for WI, SNR-PWE, MI-PWE, SINR-CC-PWE and MI-CC-PWE waveforms at $\theta_{az} = 180°$ and $\theta_{el} = 30°$.

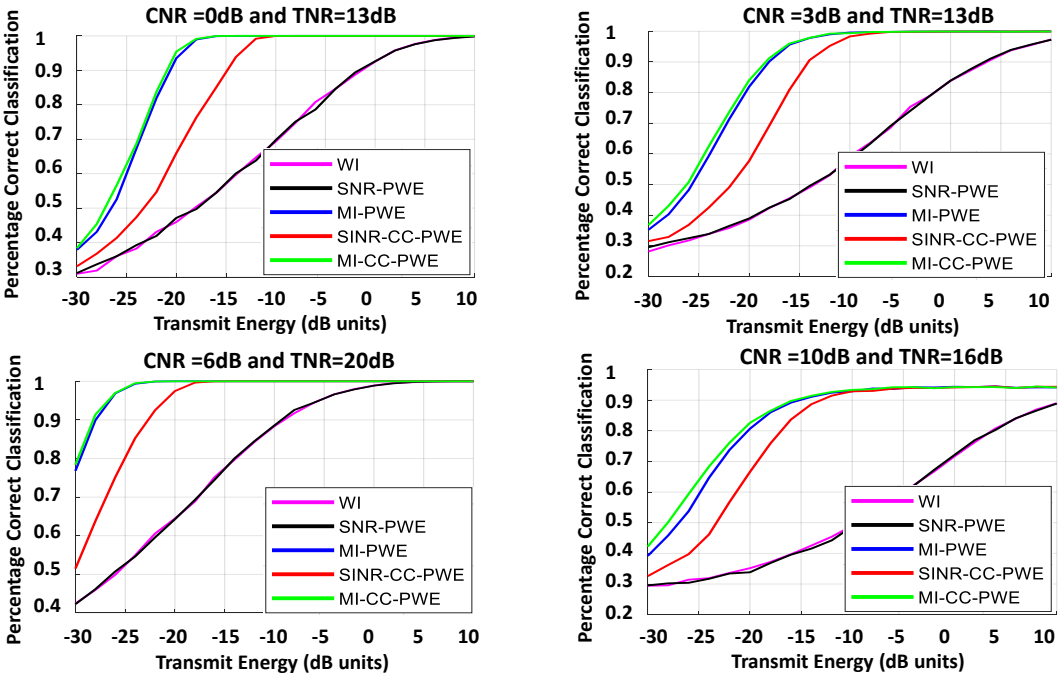

Figure 4.10. Three transmissions on ground target (narrowband clutter)—classification performance for WI, SNR-PWE, MI-PWE, SINR-CC-PWE and MI-CC-PWE waveforms at $\theta_{az} = 180°$ and $\theta_{el} = 30°$.

4.3 Target Classification Performance—Aerial Target Responses for 0° and 30° in Azimuth and 30° in Elevation

Looking at Figure 4.11, we consider the CRr closed loop system where four aerial targets are positioned at 0° and 30° in azimuth and 30° in elevation. We show in Table 4.3 the test cases (33 to 48) that are used on aerial target responses. While similar results are obtained where SINR-CC-PWE, MI-PWE and MI-CC-PWE outperform the WI and SNR-PWE, the performance is lower as compared to CST generated target responses. The classification performance of any waveform depends on the correlation of the target to the waveform as well as the clutter correlation with the target. Perhaps the CST generated EM responses correlate better with the adaptive waveforms and are not very correlated with clutter. For example, the ground-based target responses have rich frequency components as compared to aerial target responses. Moreover the aerial targets are smoother in the frequency domain, which is no doubt because of the receiver filter around the 120 MHz instantaneous bandwidth limitation of the equipment (VSG and VSA) used. But a similar conclusion is observed where MI-CC-PWE performs better against the rest of the waveforms when the CNR increases.

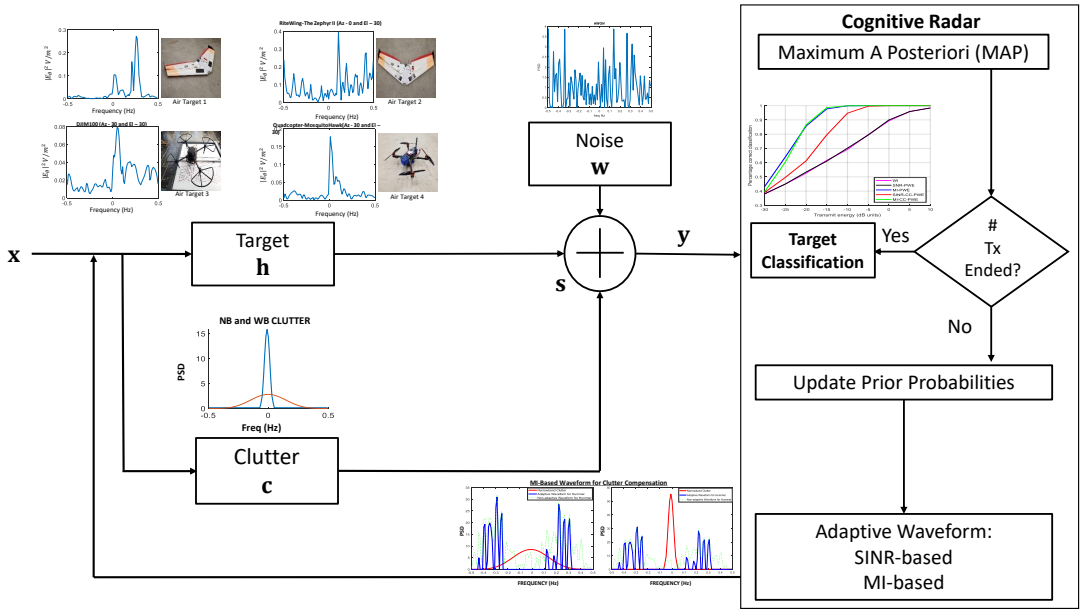

Figure 4.11. CRr closed loop diagram with aerial target responses.

Table 4.3. Test cases for aerial target responses at Az = 0° and 30° and El = 30° in signal-dependent interference

Aerial Target Responses at Az = 0° and 30°, and El = 30°					
Test Cases	Target Responses	Clutter	CNR (dB)	TNR (dB)	# of Transmission
33	Aerial Target Responses at Az = 0° and 30° and El = 30°	Wideband	0	13	1
34			3	13	1
35			6	20	1
36			10	16	1
37			0	13	3
38			3	13	3
39			6	20	3
40			10	16	3
41	Aerial Target Responses at Az = 0° and 30° and El = 30°	Narrowband	0	13	1
42			3	13	1
43			6	20	1
44			10	16	1
45			0	13	3
46			3	13	3
47			6	20	3
48			10	16	3

4.3.1 Wideband Clutter—Target Classification for One and Three Transmissions

In this section, we discuss the classification performance for test cases 33 to 40. For one transmission, the classification performance for SINR-CC-PWE, MI-PWE and MI-CC-PWE are better than WI and SNR-PWE, which are shown in Figure 4.12. MI-CC-PWE performs the best among the different types of waveforms. With three transmissions, the classification performance increases and is shown in Figure 4.13. When comparing these results with the test cases (1 to 8 and 17 to 24) under the wideband clutter, the performance is lower. With a sufficient increase in number of transmissions, the performance can be improved which shows that CRr can potentially work using actual physical targets in most clutter-limited scenarios.

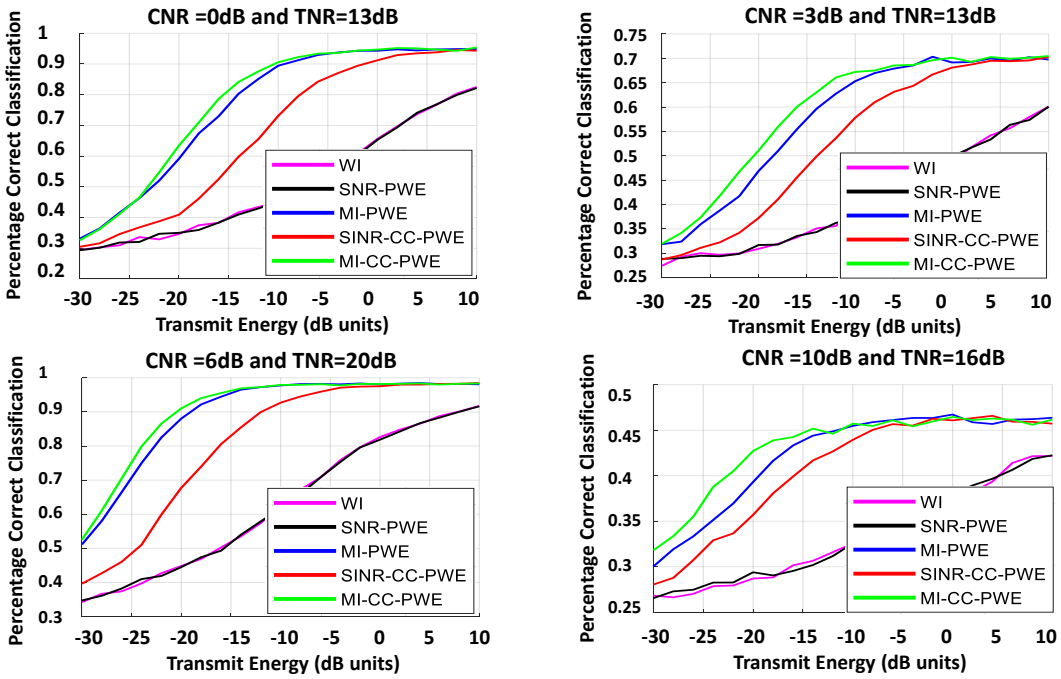

Figure 4.12. One transmission (wideband clutter)—aerial target classification performance for WI, SNR-PWE, MI-PWE, SINR-CC-PWE and MI-CC-PWE waveforms.

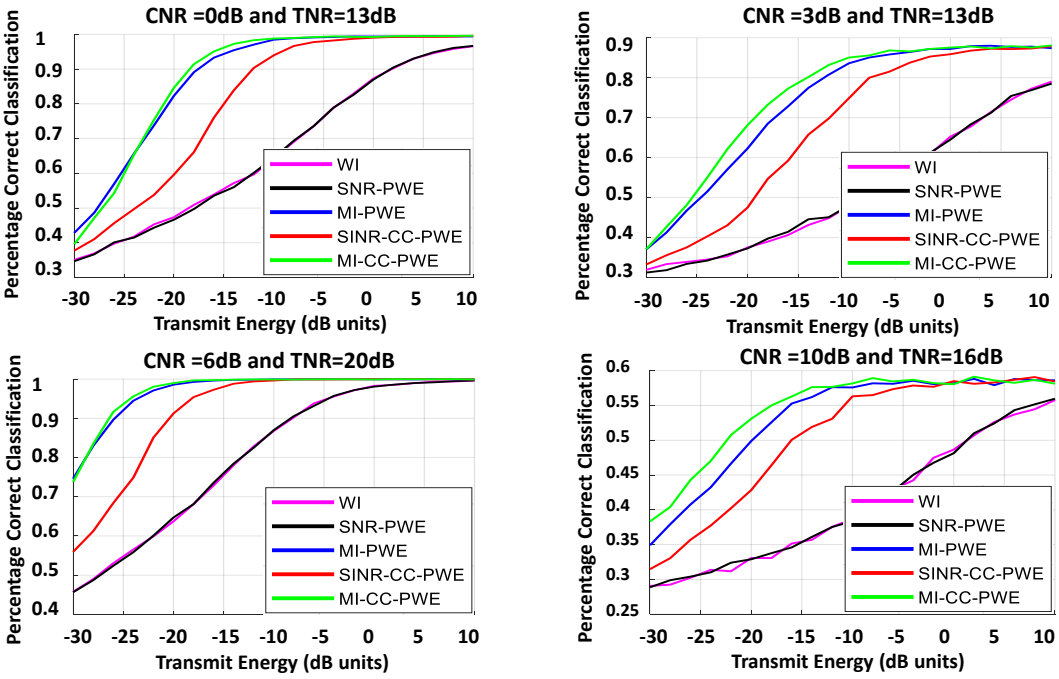

Figure 4.13. Three transmissions (wideband clutter)—aerial target classification performance for WI, SNR-PWE, MI-PWE, SINR-CC-PWE and MI-CC-PWE waveforms.

4.3.2 Narrowband Clutter—Target Classification for One and Three Transmissions

In this section, we discuss the classification performance for test cases 41 to 48. The performance results for one and three transmissions are shown in Figure 4.14 and Figure 4.15 respectively. Under narrowband clutter, the performance is better compared to wideband clutter. When we compare previous test cases under narrowband clutter (test cases 9 to 16 and 25 to 32), the performance is lower but with similar outcome where SINR-CC-PWE, MI-PWE and MI-CC-PWE outperform the WI and SNR-PWE. Again, it is noted that wideband clutter degrades the performance when compared with narrowband clutter since more total clutter energy over the entire frequency band interacts with the target response before convolution of the transmit waveform.

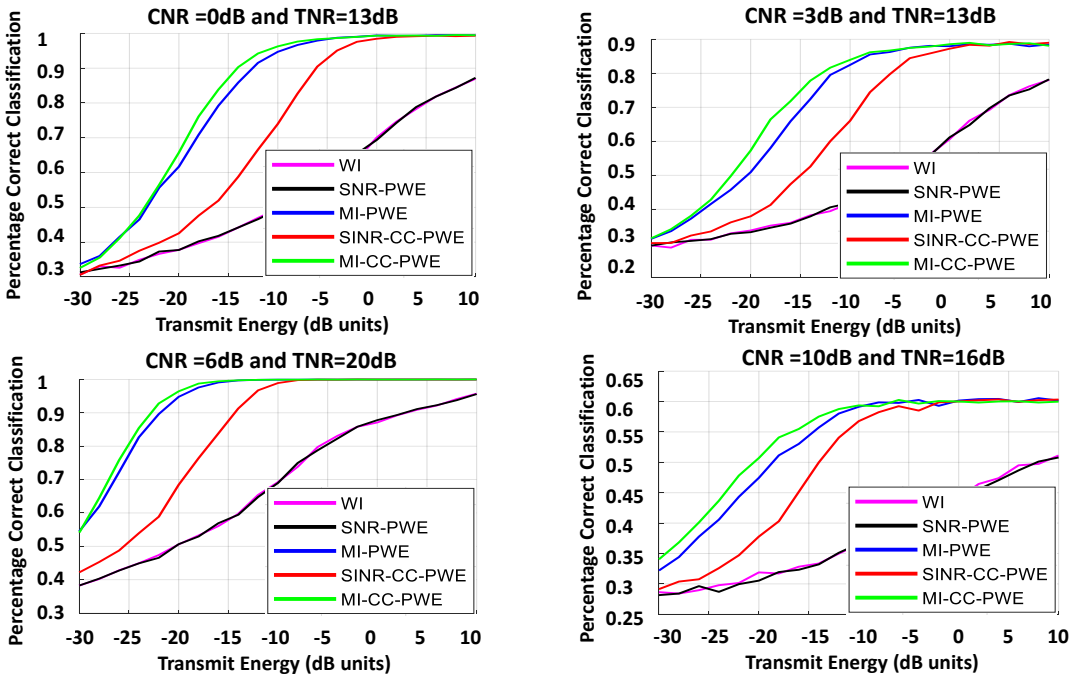

Figure 4.14. One transmission (narrowband clutter)—aerial target classification performance for WI, SNR-PWE, MI-PWE, SINR-CC-PWE and MI-CC-PWE waveforms.

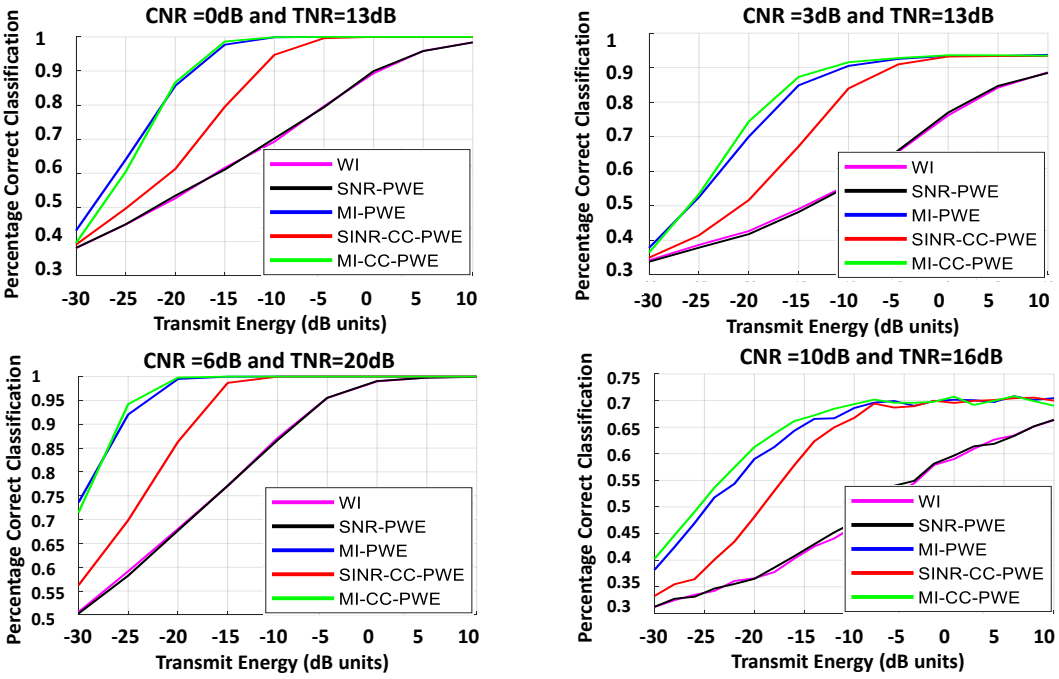

Figure 4.15. Three transmission (narrowband clutter)—aerial target classification performance for WI, SNR-PWE, MI-PWE, SINR-CC-PWE and MI-CC-PWE waveforms.

4.4 Chapter Summary

SINR-CC-PWE, MI-PWE and MI-CC-PWE outperformed the WI and SNR-PWE in all test cases. In the case of one transmission, even without the benefit of multiple transmissions, the clutter compensating waveforms already mitigated the interference effectively. With multiple transmissions, a significant improvement of performance was obtained. In all the test cases, MI-CC-PWE was the best performer when compared to all the waveforms. In addition, there was a good performance improvement for the MI-CC-PWE waveform over the MI-PWE when the CNR was large (10 dB) at three transmissions. This indicates that MI-CC-PWE will most likely perform better than MI-PWE when the system is even more clutter-limited. The SINR-CC-PWE also showed significant gain over the SNR-PWE and WI waveforms.

The target responses that were generated using CST had slightly better performance than those that were generated using the anechoic chamber method. The classification performance of any waveform depended on the correlation of the target to the waveform, as well as the clutter correlation with the target. It may be possible that the CST generated EM responses correlated better with the adaptive waveforms and are not very correlated with clutter. For instance, the ground-based target response had rich frequency components as compared to aerial target response. The aerial targets were also smoother in the frequency domain because of the receiver filter around the 120 MHz instantaneous bandwidth limitation of the equipment. However, with sufficient increase in the number of transmissions, the performance can be improved. These performance results validate the viability of using CRr under clutter-limited scenarios.

CHAPTER 5:
Conclusion and Recommendations

We presented SNR and MI-based waveforms for clutter compensation where the waveforms were able to mitigate clutter. We designed practical clutter PSD models where narrowband and wideband clutter were included in the simulation. We also generated target RCS responses at a grazing angle for realistic ground or clutter returns. Two methods were used to generate the target responses, namely via CST simulation software and using physical targets with VSG, VSA, and antennas in the anechoic chamber. We examined the ground-based and aerial target classification problems with the use of clutter-compensating transmit-adaptive waveforms in signal-dependent clutter with the use of CRr. We compared these waveforms against their uncompensated counterparts and the pulsed wideband waveform (WI) for single and three transmissions.

SINR-CC-PWE, MI-PWE and MI-CC-PWE outperformed the WI and SNR-PWE in all test cases. Without the benefit of multiple transmissions, the clutter compensating waveforms could already mitigate the interference well. With multiple transmissions, significant performance improvements were obtained. In all the 48 test cases, MI-CC-PWE was the best performer of all waveforms. There was a good performance improvement for MI-CC-PWE waveform over the MI-PWE when CNR was large (10 dB) at three transmissions. Consequently, MI-CC-PWE will most likely perform better than MI-PWE when the system is even more clutter-limited. The SINR-CC-PWE also showed significant gains over the SNR-PWE and WI waveforms. The performance was slightly lower when target responses were generated through the anechoic chamber method when compared to those generated using CST. The classification performance of any waveform depended on the correlation of the targets to the waveform as well as the clutter correlation with the target. It was likely that the CST generated EM responses correlated better with the adaptive waveforms and not very well with clutter. However, with sufficient increase in the number of transmissions, the performance could be improved.

Overall, our results showed improved target classification performance of a CRr in the presence of transmit waveform-dependent clutter when adaptive waveforms were used. It is recommended to implement a closed-loop system in hardware to validate clutter-mitigating

adaptive waveforms with cognitive radar for target classification.

List of References

[1] S. Haykin, "Cognitive radar: A way of the future," *IEEE Signal Process. Mag.*, vol. 23, no. 1, pp.30-40, Jan. 2006.

[2] M. R. Bell, "Information theory and radar waveform design," *IEEE Trans. Inform. Theory*, vol. 39, no. 5, pp.1578-1597, Sep. 1993.

[3] N. A. Goodman, P. R. Venkata and M. A. Neifeld, "Adaptive waveform design and sequential hypothesis testing for target recognition with active sensors," *IEEE J. of Sel. Topics in Sig. Proc. Mag.*, vol. 1, no. 1, pp.105-113, Jun. 2007.

[4] R. A. Romero, N. A. Goodman *et al.*, "Information-Theoretic matched waveform in signal dependent interference," *2008 IEEE Radar Conf.*, Apr 2008, Rome, Italy.

[5] R. A. Romero, "Matched waveform design and adaptive beamsteering in cognitive radar applications," *Ph.D. dissertation.*, Dept. of Elec. and Comp, Univ. of Arizona, USA, 2010.

[6] R. A. Romero, J. Bae and N. A. Goodman, "Theory and application of SNR and Mutual Information matched illumination waveforms," *IEEE Trans. Aero. and Elec. Sys.*, vol. 47, no. 2, pp.912-926, Apr. 2011.

[7] Q. J. O. Tan, R. A. Romero and D. C. Jenn, "Target recognition with adaptive waveforms in cognitive radar using practical target RCS responses," *2018 IEEE Radar Conf.*, Apr 2018, OKC, OK, USA.

[8] J. Nieh, and R. A. Romero, “Adaptive waveform for integrated detection and identification of moving extended target," *2014 48th Asilomar Conference on Signals, Systems and Computers.*, Nov 2014, Monterey, CA, USA.

[9] J. Bae and N. A. Goodman, “Automatic target recognition with unknown orientation and adaptive waveforms,” *2001 IEEE Radar Conf.*, pp.1000-1005, May 2011.

[10] Y. Z. Ma, C. Cui, B. Kim, J. Joo, S. H. Jeon, S. Nam, “Road Clutter Spectrum of BSD FMCW Automotive Radar,” *2015 IEEE Radar Conf.*, Sep 2015, Paris, France.

[11] M. A. Richards, J. A. Scheer, W. A. Holm, *Principles of Modern Radar: Basic Principles*. Edison, NJ, USA, 2010.

Initial Distribution List

1. Defense Technical Information Center
   Ft. Belvoir, Virginia

2. Dudley Knox Library
   Naval Postgraduate School
   Monterey, California